National Library of Canada
Canadian Theses Service
Ottawa, Canada
K1A 0N4

Bibliothèque nationale du Canada
Services des thèses canadiennes

CANADIAN THESES

THÈSES CANADIENNES

NOTICE

The quality of this microfiche is heavily dependent upon the quality of the original thesis submitted for microfilming. Every effort has been made to ensure the highest quality of reproduction possible.

If pages are missing, contact the university which granted the degree.

Some pages may have indistinct print especially if the original pages were typed with a poor typewriter ribbon or if the university sent us an inferior photocopy.

Previously copyrighted materials (journal articles, published tests, etc.) are not filmed.

Reproduction in full or in part of this film is governed by the Canadian Copyright Act, R.S.C. 1970, c. C-30. Please read the authorization forms which accompany this thesis.

AVIS

La qualité de cette microfiche dépend grandement de la qualité de la thèse soumise au microfilmage. Nous avons tout fait pour assurer une qualité supérieure de reproduction.

S'il manque des pages, veuillez communiquer avec l'université qui a conféré le grade.

La qualité d'impression de certaines pages peut laisser à désirer, surtout si les pages originales ont été dactylographiées à l'aide d'un ruban usé ou si l'université nous a fait parvenir une photocopie de qualité inférieure.

Les documents qui font déjà l'objet d'un droit d'auteur (articles de revue, examens publiés, etc.) ne sont pas microfilmés.

La reproduction, même partielle, de ce microfilm est soumise à la Loi canadienne sur le droit d'auteur, SRC 1970, c. C-30. Veuillez prendre connaissance des formules d'autorisation qui accompagnent cette thèse.

THIS DISSERTATION
HAS BEEN MICROFILMED
EXACTLY AS RECEIVED

LA THÈSE A ÉTÉ
MICROFILMÉE TELLE QUE
NOUS L'AVONS REÇUE

Canada

NL 339 (r. 86/01)

National Library of Canada
Canadian Theses Division
Ottawa, Canada
K1A 0N4

Bibliothèque nationale du Canada
Division des thèses canadiennes

0-315-24770-3

30

PERMISSION TO MICROFILM — AUTORISATION DE MICROFILMER

• Please print or type — Écrire en lettres moulées ou dactylographier

Full Name of Author — Nom complet de l'auteur

David C. Beamish

Date of Birth — Date de naissance	Country of Birth — Lieu de naissance
Feb 13/57	Canada

Permanent Address — Résidence fixe

6507-132 St.
Edmonton, Alta.

Title of Thesis — Titre de la thèse

Structural Dynamics Modification from Experimental Modal Analysis

University — Université

Uof A

Degree for which thesis was presented — Grade pour lequel cette thèse fut présentée

MSc (mech. eng.)

Year this degree conferred — Année d'obtention de ce grade	Name of Supervisor — Nom du directeur de thèse
1984	Dr. M.G. Faulkner

Permission is hereby granted to the NATIONAL LIBRARY OF CANADA to microfilm this thesis and to lend or sell copies of the film.

The author reserves other publication rights, and neither the thesis nor extensive extracts from it may be printed or otherwise reproduced without the author's written permission.

L'autorisation est, par la présente, accordée à la BIBLIOTHÈQUE NATIONALE DU CANADA de microfilmer cette thèse et de prêter ou de vendre des exemplaires du film.

L'auteur se réserve les autres droits de publication; ni la thèse ni de longs extraits de celle-ci ne doivent être imprimés ou autrement reproduits sans l'autorisation écrite de l'auteur.

Date	Signature
Aug 1 / 84	David Beamish

NL-91 (4/77)

THE UNIVERSITY OF ALBERTA

STRUCTURAL DYNAMICS MODIFICATION FROM EXPERIMENTAL MODAL ANALYSIS

by

© DAVID C. BEAMISH

A THESIS

SUBMITTED TO THE FACULTY OF GRADUATE STUDIES AND RESEARCH

IN PARTIAL FULFILMENT OF THE REQUIREMENTS FOR THE DEGREE

OF MASTER OF SCIENCE

DEPARTMENT OF MECHANICAL ENGINEERING

EDMONTON, ALBERTA

FALL 1984

THE UNIVERSITY OF ALBERTA

RELEASE FORM

NAME OF AUTHOR DAVID C. BEAMISH

TITLE OF THESIS STRUCTURAL DYNAMICS MODIFICATION FROM EXPERIMENTAL MODAL ANALYSIS

DEGREE FOR WHICH THESIS WAS PRESENTED MASTER OF SCIENCE

YEAR THIS DEGREE GRANTED FALL 1984

Permission is hereby granted to THE UNIVERSITY OF ALBERTA LIBRARY to reproduce single copies of this thesis and to lend or sell such copies for private, scholarly or scientific research purposes only.

The author reserves other publication rights, and neither the thesis nor extensive extracts from it may be printed or otherwise reproduced without the author's written permission.

(SIGNED) David Beamish

PERMANENT ADDRESS:

4507-132 St.
Edmonton, Alberta
T6H 3Y3

DATED July 31 1984

THE UNIVERSITY OF ALBERTA

FACULTY OF GRADUATE STUDIES AND RESEARCH

The undersigned certify that they have read, and recommend to the Faculty of Graduate Studies and Research, for acceptance, a thesis entitled STRUCTURAL DYNAMICS MODIFICATION FROM EXPERIMENTAL MODAL ANALYSIS submitted by DAVID C. BEAMISH in partial fulfilment of the requirements for the degree of MASTER OF SCIENCE.

Gary F. Faulkner

Supervisor

A. Craggs

Date July 31/84

Abstract

This study examined one of the most used techniques in structural dynamics testing - Experimental Modal Analysis (EMA). This analysis determines structural modal parameters i.e. natural frequencies, damping factors and the characteristic mode shapes of the predominant modes of vibration, from measured transfer function data.

Once these dynamic parameters were known, they could be compiled into a modal model of the structure. Modifications in the form of additions (or removal) of mass, stiffness, or damping could then be implemented analytically to predict the dynamic behavior of the modified structure. This mathematical technique called Strucural Dynamics Modification (SDM), allows for the analytical evaluation of the dynamic effects of modifications thereby dispensing with experimentation with actual physical modifications.

The first half of this study involved the validation and necessary software development for calibrated EMA and SDM. In the second half, EMA and SDM were combined and their accuracy together was evaluated. This first involved the construction of a modal model from a calibrated EMA on a test structure. Then using the modal model and SDM, predicted modification results were obtained and compared to results from an EMA on the corresponding physically modified structure.

Acknowledgements

The Author wishes to thank Dr. M.G. Faulkner for his encouragement, guidance and invaluable advice in the course of bringing this thesis to fruition.

Thanks are also extended to the Department of Mechanical Engineering in the University of Alberta and the Natural Sciences and Engineering Research Council of Canada (NSERC grant A7514) for funding the project.

Table of Contents

Chapter		Page
1.	INTRODUCTION	1
	1.1 FEA,EMA and SDM	1
	1.2 Thesis Outline	4
2.	THEORETICAL ASPECTS	7
	2.1 Modal Analysis Theory	7
	2.2 Structural Dynamics Modification Theory	15
3.	PRACTICAL ASPECTS	24
	3.1 Experimental Modal Analysis	24
	3.1.1 Data Acquisition	25
	3.1.2 Data Processing	30
	3.2 Modal Parameter Estimation	36
	3.3 Calibration	37
	3.4 Structural Dynamics Modification	40
4.	RESULTS AND DISCUSSION	44
	4.1 Calibrated EMA Validation	44
	4.2 SDM Validation	48
	4.3 Unmodified Test Structure	51
	4.4 Effects of Mass Modification	56
	4.5 Effects of Stiffness Modification	60
	4.6 Effects of Damping Modification	63
5.	CONCLUSIONS AND FURTHER STUDIES	78
REFERENCES		81

List of Tables

Table		Page
4.1	Comparison Between Theoretical and Experimental Frequencies for the Free-Free Beam	46
4.2	Comparison Between Theoretical and Experimental Mode Shapes for the Free-Free Beam	46
4.3	Theoretical Free-Free Beam Frequencies	49
4.4	Theoretical Free-Free Beam Mode Shapes	49
4.5	Summary of Predictions of Modifications to the Free-Free Beam	50
4.6	Theoretical and Predicted Frequencies for the Pinned-Pinned Configuration	52
4.7	Theoretical and Predicted Mode Shapes for the Pinned-Pinned Configuration	52
4.8	Effects on Prediction of a ±20 % Variation in the Experimental Damping Constant	70
4.9	Summary of Predictions and Tests of Modification	71
4.10	Mode 1 Mode Shapes for the z Direction	72
4.11	Mode 2 Mode Shapes for the z Direction	73
4.12	Mode 3 Mode Shapes for the z Direction	74
4.13	Mode 4 Mode Shapes for the z Direction	75
4.14	Mode 5 Mode Shapes for the z Direction	76

List of Figures

Figure		Page
2.1	A Three DOF System	17
3.1	EMA Data Acquisition Set-up	26
4.1	FRF and Coherence for the Free-Free Beam at Test Point 1	47
4.2	FRF and Coherence for the Free-Free Beam at Test Point 2	47
4.3	Original Test Structure	53
4.4	FRF and Coherence for the Original Structure at Test Point 1z	55
4.5	Original Test Structure Mode Shapes	57
4.6	FRF and Coherence for the Mass Modified Structure at Test Point 1z	59
4.7	Mass Modified Structure Synthesis Plot	59
4.8	FRF and Coherence for the Stiffness Modified Structure at Test Point 1z	62
4.9	Stiffness Modified Structure Synthesis Plot	62
4.10	Annular Rubber Shear Mount Damper	65
4.11	FRF and Coherence for the Damping Modified Structure at Test Point 1z	67
4.12	Damping Modified Structure Synthesis Plot	67

List of Plates

Plate Page

4.1 EMA Data Acquisition Set-Up and Test Structure.....77

Nomenclature

A	acceleration
$[a_k]$	residue matrix
A_k	complex constant
b	exponential window damping constant
$[B(s)]$	system matrix
c	viscous damping constant
c_k	modal damping coefficient
$[C]$	damping matrix
$[\Delta C]$	damping modification matrix
F	force
F_m	maximum frequency
F_s	sampling frequency
Δf	frequency resolution
$\{f\}$	forcing vector
$F(\Omega)$	modified structure complex eigenvalue function
G_{ff}	forcing power spectrum
G_{rr}	response power spectrum
G_{nn}	noise power spectrum
G_{rf}	cross spectrum
G_{nf}	noise cross spectrum
H_A	actual FRF
H_c	calibration function
H_I	measured calibration block FRF
H_M	measured structure FRF
$[H(s)]$	transfer function matrix
$[I]$	identity matrix

k	stiffness value
k_i	modal stiffness coefficient
k_x, k_y, k_z	respective direction stiffnesses
$[K]$	stiffness matrix
$[\Delta K]$	stiffness modification matrix
$\{l\}$	local modification position vector
m	mass value
m_c	calibration block mass
m_i	modal mass coefficient
$[M]$	mass matrix
$[\Delta M]$	mass modification matrix
N	number of time sample points
p_i	system pole
s	complex variable
S_n	Fourier tranformed noise signal
S_f	Fourier transformed forcing signal
S_r	Fourier transformed response signal
Δt	sampling interval
T	time record period
$\{u_i\}$	modal vector
$w(t)$	window function
$\{x\}$	displacement vector
X, Y	displacement values
$\{z\}$	modal coordinates vector
α, β, γ	respective physical modification values
γ^2	coherence function
σ_i	damping coefficient

$\{\phi\}$	modal matrix row vector
ω_k	natural frequency coefficient
ω_f	forcing frequency
$[\Phi]$	modal matrix
Ω	modified structure complex eigenvalue

1. INTRODUCTION

1.1 FEA,EMA and SDM

An important consideration in the design and operation of mechanical structures and machines is a knowledge of their dynamic characteristics. These characteristics are determined by the interaction of the mass, elastic and damping properties of the system and can be expressed through modal parameters. These modal parameters include the damping, natural frequencies and mode shapes of the predominant modes of vibration and can be found either analytically or experimentally. Once known, the modal parameters can be compiled to form a complete system dynamic model or modal model. This model then allows the prediction of the dynamic response of the structure or machine due to any applied set of forces.

Simple systems can be described by continuous models where the modal parameters are derived from the formulation of one or more differential equations. Often however, the complexity of the system is such that approximations such as discretization of a continuous structure is used. In this case, the actual system is modelled by a set of discrete masses or rigid bodies coupled by springs and dampers. Application of the basic equations of dynamics will then result in a system of second order differential equations which can be solved simultaneously for the modal parameters.

More recently for complex structures, the dynamics have been calculated by means of Finite Element Analysis (FEA) (for example Zienkiewicz [32]). FEA involves the discretization of a mechanical structure into small elements. The structures dynamic equations are then assembled as a combination of the individual elements equations of motion and boundary conditions. To accurately model the structure, many elements and thus hundreds or thousands of degrees-of-freedom may be required. Because of the size and complexity of these models, they can be expensive and time consuming to both develop and use. In addition, it is often found that due to an insufficient number of elements and unrepresentative boundary conditions that the model does not accurately describe the actual situation. Because of these problems, validation of analytical models is often performed using experimental dynamic testing.

One of the most popular forms of dynamic testing in recent years is Experimental Modal Analysis (EMA). For a detailed explanation of the subject see Richardson [24]. This analysis is based on obtaining simultaneous excitation and response measurements at points of interest on the structure. By dividing the Fourier transform of the response by the Fourier transform of the excitation, a transfer function between the various response and excitation points is formed. The modal parameters are then extracted by curve fitting an analytical expression to the experimentally

determined transfer functions. The modal parameters can then be compiled to form an experimental modal model.

Experimental modal models have several advantages over the analytical. The number of degrees-of-freedom (m) in the finite element model dictates the models size of m x m. Therefore, m, or hundreds to thousands of simultaneous equations must be solved. Although the solution results in m modes, the large majority of them are outside the frequency range of interest. In the experimental case, the curve fit results in n modes in the required range. Thus the model size can be considerably smaller (n x n). This means that for the experimental model, computation is faster, memory requirements are less, and thus a smaller computer can be used. The second advantage is that an experimental model represents the actual structure. The third is that an experimental model can be obtained for structures too complex to be easily modelled analytically.

The combination of analytical and experimental analysis, when possible, represents a most powerful tool in assessing a structures dynamics. By direct comparison between the experimental and analytical modal model, shortcomings or errors in each can be detected. It then becomes possible to either re-model portions of the finite element model or re-measure data at particular points on the structure to form a set of more consistent results.

Once the modal model is acceptable, the effects of proposed changes to the structure to either optimize the

dynamic behavior or alter it to alleviate problems can be examined using a technique called Structural Dynamics Modification (SDM). This technique developed by engineers at Structural Measurement Systems Inc., is outlined in some detail in Formenti and Welaratna [6]. SDM uses either an experimental or analytical model to analytically evaluate the effects of modifications to the structure in the form of stiffeners, dampers or point masses. The technique is very concise and thus numerous modification proposals can be investigated quickly. This fact takes on immense importance especially in FEA. Because of the complexity of the structure usually modelled, placement and amount of modification is not obvious and thus the evaluation of modifications can involve a fair amount of trial and error. To alter and run a finite element model for each change can be time consuming and expensive. However, by first finding a salient change quickly and easily using SDM, the finite element model could then be run to further detail the effect of the particular modification.

1.2 Thesis Outline

The fundamental objective of this study was to extend the basic EMA software package developed by Fyfe [7] to enable SDM. This involves further software development as well as transfer function calibration and the introduction of the SDM technique.

Chapter two summarizes modal analysis and the relationship between theory and experiment. Also included is the method of extracting modal parameters from transfer function data. Further theoretical investigations extend the concepts to the SDM technique and its development using the modal model.

Chapter three discusses the practical aspects of using EMA and SDM. These considerations include the relevant fundamentals of signal analysis and hardware requirements in relation to data acquisition and data processing. This leads into a discussion of the curve fitting process and transfer function calibration. As well, practical considerations of the SDM technique involve the use of the Newton-Raphson technique in determining the modified structure eigenvalues.

The fourth chapter discusses the results obtained from the separate validation and combined evaluation of calibrated EMA and SDM. As the accuracy of the predicted dynamic effects of modifications on a structure using SDM depends on the accuracy of modal parameter estimates obtained using calibrated EMA results, this chapter first examines modal parameter estimation accuracy by comparing results obtained from an EMA on a free-free beam to those predicted from theory. SDM accuracy was checked by making various analytical modifications to the theoretical model for the free-free beam and comparing these to the corresponding theoretical results. To evaluate the combination of EMA and SDM, modal parameters were obtained

for a test structure in which the modal parameters were obtained only from EMA. Then using SDM, predictions of the modified dynamics for mass, stiffness and damping changes were compared to EMA results obtained from the physically modified structure for each modification.

The last chapter briefly summarizes many of the results, assumptions and improvements as well as future considerations.

2. THEORETICAL ASPECTS

A continuous, elastic structure can be discretized into a system of lumped parameter elements. The motion of this system can be approximated by a set of simultaneous linear second order differential equations. In the time domain, these equations would be of the form:

$$[M]\{\ddot{x}\} + [C]\{\dot{x}\} + [K]\{x\} = \{f\} \qquad (2.1)$$

where [M], [C] and [K] are the mass, damping and stiffness matrices, assumed to be real and symmetric, {f} is the applied force vector and {x} is the resulting displacement vector.

2.1 Modal Analysis Theory

Taking the Laplace transform of equation (2.1) and assuming zero initial conditions gives:

$$[[M]s^2 + [C]s + [K]]\{x(s)\} = \{f(s)\}$$

which can also be written as:

$$[B(s)]\{x(s)\} = \{f(s)\} \qquad (2.2)$$

where: $[B(s)] = [M]s^2 + [C]s + [K]$

The matrix [B(s)] is called the system matrix and its

inverse is referred to as the transfer matrix, [H(s)]:

$$[H(s)] = [B(s)]^{-1} = \frac{\text{Adj } [B(s)]}{\text{Det } [B(s)]} \tag{2.3}$$

Equation (2.2) and equation (2.3) thus lead to:

$$[H(s)]\ \{f(s)\} = \{x(s)\} \tag{2.4}$$

The Laplace variable, s, is complex and can thus be represented by its real and imaginary parts as $s = \sigma + j\omega$. Therefore, an s-plane can be defined where σ is referred to as the damping axis and $j\omega$ as the frequency axis. The transfer function matrix [H(s)] is complex since it is a function of s, and therefore its magnitude can be plotted on the s-plane. At particular points on the s-plane called poles, the magnitude of the transfer function goes to infinity. The poles occur as complex conjugates where each pair represents a particular resonance or mode of vibration. As a result, for an n degree-of-freedom system, there are n-pole pairs describing the damping and frequency of n modes. Each pole pair can be expressed at a particular mode (k) as:

$$P_k = \sigma_k + j\omega_k \qquad P_k^* = \sigma_k - j\omega_k$$

where: '*' denotes the complex conjugate, σ_k is the damping coefficient (negative for stable systems) and ω_k is the

natural frequency.

From equation (2.3) it is clear that the elements of [H(s)] are rational functions in s. Therefore they may be written in partial fraction form as:

$$[H(s)] = \sum_{k=1}^{2n} \frac{[a_k]}{s - p_k} = \sum_{k=1}^{n} \left[\frac{[a_k]}{s - p_k} + \frac{[a_k^*]}{s - p_k^*} \right] \qquad (2.5)$$

where: $[a_k]$ is a complex residue matrix containing spatial behavior information at each mode.

Premultipling equation (2.5) by $(s-p_k)[B(s)]$ gives:

$$(s - p_k)[B(s)][H(s)] = (s - p_k)[B(s)] \sum_{k=1}^{2n} \frac{[a_k]}{s - p_k}$$

At a mode, $s = p_k$. Substituting this expression into the previous one results in:

$$[B(p_k)][a_k] = 0$$

It can also be shown in a similiar manner by postmultiplying by [B(s)] instead, that:

$$[a_k][B(p_k)] = 0$$

Therefore, the rows and columns of $[a_k]$ must be linear combinations of homogenous solution vectors $\{u_k\}$ such that:

$$[B(p_k)]\ \{u_k\} = \{0\}$$

The $\{u_k\}$ vectors are defined as the mode shape at the pole, p_k. The rows and columns of $[a_k]$, must then be a scalar multiple of the vectors $\{u_k\}$. Thus the matrix $[a_k]$ can be expressed as:

$$[a_k] = A_k\{u_k\}\{u_k\}^T \tag{2.6}$$

where 'T' denotes the transpose and A_k is a complex scalar. Substituting equation (2.6) into equation (2.5) yields:

$$[H(s)] = \sum_{k=1}^{n} \left[\frac{A_k\{u_k\}\{u_k\}^T}{s - p_k} + \frac{A_k^*\{u_k^*\}\{u_k^*\}^T}{s - p_k^*} \right] \tag{2.7}$$

Equation (2.6) and (2.7) show that every row and column of the residue matrix and thus the transfer function matrix, is comprised of the mode shape vector multiplied by a different element of itself. Therefore, only one row or column is needed at each mode. Equation (2.7) also shows that the transfer function matrix can be built entirely from the modal parameters (natural frequency, damping factor and mode shapes) and that it completely describes the modal model.

Further reduction of the problem can be accomplished by computing the Laplace transform along the frequency axis where $s = j\omega$. This subclass of the Laplace transform called the Fourier transform results in a particular type of transfer function referred to as the frequency response function. Since the transfer function is represented analytically, the entire s-plane can be generated from the

frequency response function if required.

In order to measure the frequency response function, it is possible to rewrite equation (2.4) in matrix form. Assuming a two degree-of-freedom system this results in:

$$\begin{bmatrix} h_{11}(s) & h_{12}(s) \\ h_{21}(s) & h_{22}(s) \end{bmatrix} \begin{Bmatrix} f_1(s) \\ f_2(s) \end{Bmatrix} = \begin{Bmatrix} x_1(s) \\ x_2(s) \end{Bmatrix} \qquad (2.8)$$

where $s = j\omega$.

Since only one row or column of the transfer function matrix is required, consideration of the first equation in equation (2.8) serves as an example:

$$x_1(s) = h_{11}(s)f_1(s) + h_{12}(s)f_2(s) \qquad (2.9)$$

To form the first row of the transfer function matrix, the response is measured only at the first point while the excitation is applied and measured at one point at a time to all points of interest. The first element in the first row can be found by exciting the structure at the first point while simultaneously measuring the response at the first point. Equation (2.9) then gives:

$$h_{11}(\omega) = \frac{x_1(\omega)}{f_1(\omega)} \qquad h_{11}(\omega) = h_{11}(s) \Big|_{s = j\omega}$$

The second element in the first row can be found by exciting the structure at the second point while simultaneously measuring the response at the first point. Thus equation

(2.9) gives:

$$h_{12}(\omega) = \frac{x_1(\omega)}{f_2(\omega)} \qquad h_{12}(\omega) = h_{12}(s) \Big|_{s = j\omega}$$

Any other row or column can be built in a similar manner and each element is formed from taking the Fourier transform of the response and dividing by the Fourier transform of the excitation force.

The modal parameters can then be estimated from the measured frequency response function by curve fitting each transfer function in a row or column of the transfer function matrix using equation (2.5) for $s = j\omega$. This curve fitting process is discussed in the following chapter.

As will be shown in the next section of this chapter, structural modifications are accomplished by a coordinate transformation to modal coordinates. Thus the following describes the formulation of the modal matrices derived from the modal parameters.

Since only one row or column of the residue matrix $[a_k]$ is required, consider for example the jth column. From equation (2.6):

$$\{a_{kj}\} = A_k\{u_k\}u_{kj} = A_k u_{kj}\{u_k\} \qquad (2.10)$$

where u_{kj} is the jth element of $\{u_k\}$.

The scalar, A_k, can be expressed from equation (2.10) as:

$$A_k = \frac{|a_{kj}|}{u_{kj}|u_k|} = \frac{(\{a_{kj}\}^T\{a_{kj}\})^{1/2}}{u_{kj}(\{u_k\}^T\{u_k\})^{1/2}} \qquad (2.11)$$

where | | denotes the vector magnitude.

The value of A_k clearly depends on the normalization of the modal vector $\{u_k\}$. Assuming measurements are available from the jth row or jth column of the transfer function matrix, the modal vector may be shown as:

$$\{u_k\} = \frac{1}{a_{kjj}} \{a_{kj}\} \qquad (2.12)$$

where a_{kjj} is the jth row, jth column element of $[a_k]$.

Equation (2.12) can be rearranged into:

$$a_{kjj} = \frac{|a_{kj}|}{|u_k|}$$

Substituting into equation (2.11) and recognizing that u_{kj} is equal to unity gives the simplified expression:

$$A_k = a_{kjj}$$

Recognizing that A_k has the dimensions, sec/mass, and from the assumption that the mass, stiffness and damping matrices are real, Richardson and Potter [26] defined the modal mass, damping and stiffness as:

$$m_k = \frac{1}{-(A_k p_k^* + A_k^* p_k)}$$

$$c_k = \frac{p_k + p_k^*}{A_k p_k^* + A_k^* p_k}$$

$$k_k = \frac{p_k p_k^*}{A_k p_k^* + A_k^* p_k}$$

For the normal mode case (zero damping), the system matrix is real symmetric and thus A_k and p_k are purely imaginary and the vector $\{u_k\}$ is real valued. Therefore:

$$A_k = -A_k^*$$

$$p_k = -p_k^*$$

$$\{u_k\} = \{u_k^*\}$$

As a result, the modal mass, stiffness and damping assume the form:

$$m_k = \frac{1}{2 A_k p_k} \qquad (2.13)$$

$$c_k = 0 \qquad (2.14)$$

$$k_k = \frac{P_k}{2 A_k} \qquad (2.15)$$

and the transfer matrix becomes:

$$[H(s)] = \sum_{k=1}^{n} \left[\frac{\{u_k\}\{u_k\}^T}{m_k s^2 + k_k} \right]$$

2.2 Structural Dynamics Modification Theory

Structural Dynamics Modification is a technique developed by Structural Measurement Systems Inc.. Following is the adaptation of this technique from Formenti and Welaratna [6].

The removal of the forcing function from equation (2.1) represents the free motion of a damped system expressed as:

$$[M]\{\ddot{x}\} + [C]\{\dot{x}\} + [K]\{x\} = \{0\}$$

Modifications to the system can be implemented locally using a technique called Diakoptics or eigenvalue modification. This technique was initially developed by Kron [14], Simpson and Tabarrok [28] and Weissenburger [31] and extended by Pomazal [18], Hallquist [8] and Hallquist and Snyder [9].

Local modifications with respect to the physical system may be shown as:

$$[\Delta M] = \alpha\{1\}\{1\}^T \qquad [\Delta C] = \beta\{1\}\{1\}^T \qquad [\Delta K] = \gamma\{1\}\{1\}^T$$

where α, β and γ are the values of the respective changes in physical units. The vector {1} locates the change in physical coordinates.

This procedure allows modifications in the form of additions or removals of point masses, scalar dampers and/or springs applied from a point to ground and scalar dampers and/or springs applied between two points. This same procedure also enables the joining together of substructures by scalar dampers and/or springs.

To illustrate the local modification procedure, a simple 3 DOF discrete system as shown in figure 2.1 can be used. Since the system coordinates are in a static coupling form, modifications can be made in physical coordinates in this case.

Letting $k_1 = 0$, the following stiffness matrix is generated:

$$\begin{bmatrix} k_2 & -k_2 & 0 \\ -k_2 & (k_2 + k_3) & -k_3 \\ 0 & -k_3 & (k_3 + k_4) \end{bmatrix}$$

In order to regenerate the original stiffness matrix, the local modification procedure can be applied such that k_1 is attached from point 1 to ground. Thus, the modification matrix would be:

$$[\Delta k] = k_1 \{1\}\{1\}^T$$

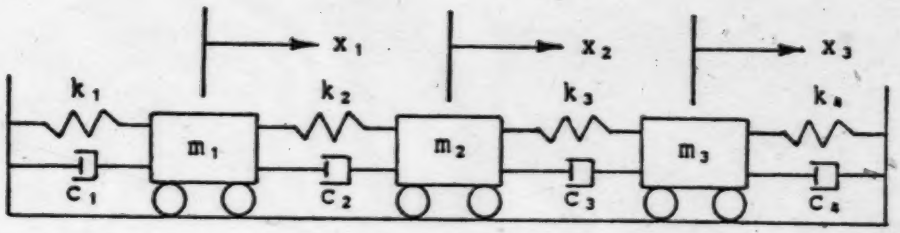

$$\begin{bmatrix} m_1 & 0 & 0 \\ 0 & m_2 & 0 \\ 0 & 0 & m_3 \end{bmatrix} \begin{Bmatrix} \ddot{x}_1 \\ \ddot{x}_2 \\ \ddot{x}_3 \end{Bmatrix} + \begin{bmatrix} (c_1 + c_2) & -c_2 & 0 \\ -c_2 & (c_2 + c_3) & -c_3 \\ 0 & -c_3 & (c_3 + c_4) \end{bmatrix} \begin{Bmatrix} \dot{x}_1 \\ \dot{x}_2 \\ \dot{x}_3 \end{Bmatrix}$$

$$+ \begin{bmatrix} (k_1 + k_2) & -k_2 & 0 \\ -k_2 & (k_2 + k_3) & -k_3 \\ 0 & -k_3 & (K_3 + k_4) \end{bmatrix} \begin{Bmatrix} x_1 \\ x_2 \\ x_3 \end{Bmatrix} = \begin{Bmatrix} 0 \\ 0 \\ 0 \end{Bmatrix}$$

Figure 2.1 A Three DOF System

where the {1} vector assumes the form:

$$\{1\} = \begin{Bmatrix} 1 \\ 0 \\ 0 \end{Bmatrix}$$

and:

$$k_1 \{1\}\{1\}^T = \begin{bmatrix} k_1 & 0 & 0 \\ 0 & 0 & 0 \\ 0 & 0 & 0 \end{bmatrix}$$

Adding this matrix to the $k_1 = 0$ matrix regenerates the original matrix.

Supposing instead that $k_2 = 0$, then the following stiffness matrix would result:

$$\begin{bmatrix} k_1 & 0 & 0 \\ 0 & k_3 & -k_3 \\ 0 & -k_3 & (k_3 + k_4) \end{bmatrix}$$

To regenerate the original stiffness matrix, the modification would take the form:

$$[\Delta K] = k_2\{1\}\{1\}^T$$

where this time a spring is added between point 1 and point 2 so that the {1} vector would take the form:

$$\{1\} = \begin{Bmatrix} 1 \\ -1 \\ 0 \end{Bmatrix}$$

and:

$$k_2\{1\}\{1\}^T = \begin{bmatrix} k_2 & -k_2 & 0 \\ -k_2 & k_2 & 0 \\ 0 & 0 & 0 \end{bmatrix}$$

By adding this matrix to the $k_2 = 0$ matrix yields the original matrix.

Since the mass, damping and stiffness changes are being implemented at the same point, the modified system equation would take the form:

$$[M]\{\ddot{x}\} + [C]\{\dot{x}\} + [K]\{x\} + [\Delta M]\{\ddot{x}\} + [\Delta C]\{\dot{x}\} + [\Delta K]\{x\} = \{0\} \quad (2.16)$$

Instead of using the Laplace transform as before to obtain the solution vector {x}, it is also possible to simply assume a solution of the form:

$$\{x\} = \{\dot{x}\}e^{\Omega t}$$

Substitution into equation (2.16) yields:

$$[\Omega^2[M] + \Omega[C] + [K] + (\alpha\Omega^2 + \beta\Omega + \gamma)\{1\}\{1\}^T]\{\dot{x}\} = \{0\} \quad (2.17)$$

Because of practical measurement considerations (to be discussed in the next chapter), a real mode model with proportional damping (as opposed to a complex model) is assumed. The mode shapes $\{u_k\}$ for the system are therefore

real and can thus be used directly in making a coordinate transformation to uncouple the equations of motion. As will be shown below, by also normalizing the mode shapes to unit modal mass, the uncoupled equations can be written solely in terms of the modal parameters.

In order to normalize the mode shapes to unit modal mass, the mode shape vector $\{u_k\}$ is scaled such that it would take the form:

$$\{u_k\}/\sqrt{m_k}$$

where m_k is the modal mass obtained from equation (2.13). The mode shape vector is now in the appropriate form to uncouple the equations of motion in terms of the modal parameters. This is done by a coordinate transformation to modal coordinates using the modal matrix:

$$\{x\} = [\Phi]\{z\} \qquad (2.18)$$

where:

$$[\Phi] = \left[\frac{\{u_1\}}{\sqrt{m_1}}, \frac{\{u_2\}}{\sqrt{m_2}}, \ldots \frac{\{u_n\}}{\sqrt{m_n}}\right]$$

and $\{z\}$ are the modal coordinates. Substitution of equation (2.18) into equation (2.17) and premultiplying by $[\Phi]^T$ gives:

$$[\Omega^2[\Phi]^T[M][\Phi] + \Omega[\Phi]^T[C][\Phi] + [\Phi]^T[K][\Phi] + (\alpha\Omega^2 + \beta\Omega + \gamma)[\Phi]^T\{1\}\{1\}^T[\Phi]]\{z\} = \{0\}$$

Since the system was assumed to be proportionally damped and utilizing mode shape orthogonality, the equations of motion in modal coordinates become:

$$[\Omega^2 \lceil I \rfloor + \Omega\lceil 2\sigma \rfloor + \lceil \sigma^2 + \omega^2 \rfloor + (\alpha\Omega^2 + \beta\Omega + \gamma)\{\phi\}\{\phi\}^T]\{z\} = \{0\} \quad (2.19)$$

where $\{\phi\} = [\Phi]^T\{1\}$ and:

σ - original structure damping coefficient

ω - original structure natural frequency

Ω - modified structure complex eigenvalue

$\{z\}$ - modified structure eigenvector

Since the equations are uncoupled, it is possible to write the ith equation as:

$$(\Omega^2 + 2\sigma_i\Omega + (\sigma_i^2 + \omega_i^2))\frac{z_i}{\phi_i} = -(\alpha\Omega^2 + \beta\Omega + \gamma)\sum_{k=1}^{n} \phi_k z_k \quad (2.20)$$

Therefore:

$$(\Omega^2 + 2\sigma_1\Omega + (\sigma_1^2 + \omega_1^2))\frac{z_1}{\phi_1} = (\Omega^2 + 2\sigma_2\Omega + (\sigma_2^2 + \omega_2^2))\frac{z_2}{\phi_2} \quad (2.21)$$

$$= \ldots$$

$$= (\Omega^2 + 2\sigma_n\Omega + (\sigma_n^2 + \omega_n^2))\frac{z_n}{\phi_n}$$

$$= -(\alpha\Omega^2 + \beta\Omega + \gamma)\sum_{k=1}^{n} \phi_k z_k$$

From equation (2.21) it is clear that an expression for the kth element of the vector {z} can be determined in terms of any ith element. This fact leads to:

$$z_k = \frac{z_i}{\phi_i}(\Omega^2 + 2\sigma_i\Omega + (\sigma_i^2 + \omega_i^2))\cdot \frac{\phi_k}{(\Omega^2 + 2\sigma_k\Omega + (\sigma_k^2 + \omega_k^2))} \qquad (2.22)$$

Substituting equation (2.22) into (2.20) yields:

$$(\Omega^2 + 2\sigma_i\Omega + (\sigma_i^2 + \omega_i^2))\frac{z_i}{\phi_i}$$

$$= -(\alpha\Omega^2 + \beta\Omega + \gamma)\sum_{k=1}^{n}\frac{z_i}{\phi_i}(\Omega^2 + 2\sigma_i\Omega + (\sigma_i^2 + \omega_i^2))\cdot \frac{\phi_k^2}{(\Omega^2 + 2\sigma_k\Omega + (\sigma_k^2 + \omega_k^2))}$$

which reduces to:

$$\frac{-1}{(\alpha\Omega^2 + \beta\Omega + \gamma)} = \sum_{k=1}^{n} \frac{\phi_k^2}{(\Omega^2 + 2\sigma_k\Omega + (\sigma_k^2 + \omega_k^2))} \qquad (2.23)$$

Equation (2.23) represents the modified systems characteristic equation. Once the eigenvalues have been solved from this equation, the eigenvectors can be computed

from equation (2.22) to within an arbitrary constant, A_i. The kth element of the ith mode is then:

$$z_k = A_i \frac{\phi_k}{(\Omega_i^2 + 2\sigma_k\Omega_i + (\sigma_k^2 + \omega_k^2))} \qquad (2.24)$$

The constant A_i is found by normalizing the modified mode shapes to unit modal mass so that:

$$\{z_i\}^T\{z_i\} = 1$$

Since the modified mode shapes are in terms of modal coordinates, the transformation back to physical coordinates can be accomplished using equation (2.18). As a result, for the ith mode:

$$\{x_i\} = [\Phi]\{z_i\}$$

Thus, the eigenvalues and eigenvectors of the modified system are determined using the original modal parameters and applying the assumption of a real mode model with proportional damping. The implementation of this procedure is shown in the next chapter.

3. PRACTICAL ASPECTS

In the previous chapter, the frequency response functions, which are the basis of determining modal information, were obtained by dividing the Fourier transforms of the simultaneously measured excitation and response time domain signals. While theoretically this is straight forward, in a practical sense there are several difficulties and inaccuracies which must be overcome. This chapter therefore begins by outlining the practical problems of modal analysis associated with signal analysis and hardware for data acquisition, data processing and calibration. The final section deals with computing considerations for the practical aspects of SDM necessary in obtaining modified eigenvalues and eigenvectors from the modal parameters.

3.1 Experimental Modal Analysis

EMA relies on broadband excitation signals in which most of the modes of interest are excited simultaneously. The various classes of these signals include transient, random and swept sine. In this study, the transient method using a hand held hammer was chosen because of its easy implementation in various situations. The other two methods rely on the use of shakers and thus are more cumbersome. The transient method, unfortunately, has two major disadvantages. If a structure is large and heavily damped, it becomes difficult to adequately excite it in this way.

Also the method is inadequate when nonlinearities are present since the spectrum level cannot be precisely controlled. The test structures in this study, however, were small and lightly damped with little nonlinearity so that these factors did not present a problem.

3.1.1 Data Acquisition

The experimental set-up for data acquisition using the transient method is shown in figure 3.1. Each component will be discussed below in relation to its significance in the signal analysis process and its use.

The hammer represents the basic component in the transient method. Hammer weight and tip hardness determine the excitation force frequency content. Since the structures considered were relatively small, a light weight hammer of about 200 gm was chosen. The load cell mounted in the head of the hammer to measure the force, had a sensitivity of about 2.2 mV/N. Structural frequencies below 1000 Hz were to be examined and therefore the tip was chosen so as to concentrate most of the energy in this range. As a result, a hard rubber tip was used, which resulted in an excitation force spectrum that was flat (±3 dB) to about 1300 Hz. While the input force was being measured by the hammer-mounted load cell, the response was simultaneously measured by an accelerometer. An initial accelerometer used came with the hammer kit, but was found to cause accelerometer loading errors. The accelerometer's 26 gm weight was substantial

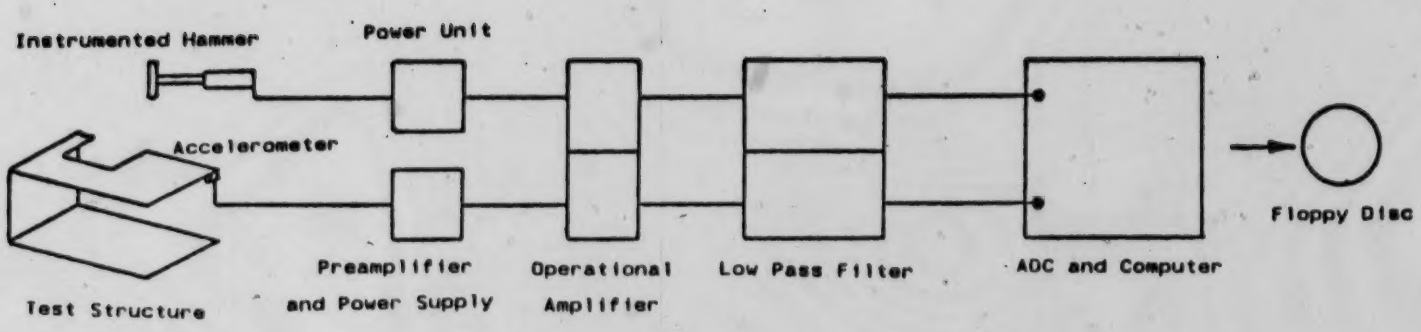

Instrumented Hammer - PCB Piezotronics Model 208 A03

Power Unit - PCB Piezotronics Model 480 A

Accelerometer - Bruel & Kjaer Type 4344

Preamplifier - Bruel & Kjaer Type 2616

Power Supply - Hewlett-Packard Model 6213 A

Operational Amplifier - custom

Low Pass Filter - Krohn-Hite Model 3342

ADC and Computer - DEC MINC-23

Figure 3.1 EMA Data Acquisition Set-up

enough to affect the dynamics of the test structures. Thus a much lighter accelerometer (2 gm) was used. While this lower mass gave a small accelerometer loading error, it also reduced the output sensitivity from 10 mV/g to 2.37 mV/g.

Since analysis or processing of the excitation and response time waveforms produced by the hammer and accelerometer requires digital computation, the signals must be digitized and limited to a finite period. The discrete waveforms thus have a finite resolution (Δt) based on the number of samples (N) and the period (T). This time domain relationship can be expressed as:

$$T = N\Delta t$$

In order to transform the digitized waveforms to the frequency domain, the Discrete Fourier Transform (DFT) is used. The algorithm which accomplishes this task, is called the Fast Fourier Transform (FFT). The resulting frequency waveforms are complex quantities and are thus made up of two parts, namely the magnitude and phase. Therefore, N time domain samples will yield N/2 complex frequency domain samples. This frequency domain relationship may be shown as:

$$F_m = \frac{N}{2}\Delta f$$

where F_m is the maximum value of the frequency in the frequency range of interest and Δf is the frequency

resolution according to the relation:

$$\Delta f = \frac{1}{T}$$

Rearrangement of the previous three relations results in:

$$F_m = \frac{N}{2} \cdot \frac{1}{T} = \frac{1}{2\Delta t} = \frac{F_s}{2}$$

where F_s is the sampling frequency. N is a fixed value in the FFT algorithm (typically N = 1024). Therefore to extend the frequency range of interest, the sampling frequency is increased and thus the time period is shortened. Note then that this also results in lower frequency resolution.

From the previous equation, it can be seen that the sampling frequency, F_s, must be twice the maximum frequency. This relationship is referred to as Shannon's Sampling Theorem. If F_s is less than twice, a problem called aliasing can occur. This problem refers to the fact that signals of frequency greater than the difference between F_s and F_m will overlap or alias in the frequency range of interest. However, by setting F_s at least twice F_m, the difference would then cause the alias signals to fall above the F_m limit. Since aliasing can also occur due to stray signals from surrounding sources, a low pass filter is used to ensure that the frequency range is limited. Because of the finite filter roll-off (a characteristic of all filters) the cut-off set at F_m does not ensure that all higher

frequencies are completely rejected. Signals occurring in the roll-off band might not be entirely attenuated by the time they alias in the frequency range of interest. To account for this effect, the sampling frequency is usually raised to 2.56 times the maximum frequency. The filter used in this study had a roll-off rate of 96 dB/octave. Thus, if $F_s = 2.56F_m$, then alias signals would be attenuated by approximately 62 dB. This is more than enough since the entire range considered in this study was 60 dB.

Digitizing is done by an analog to digital converter (ADC). The type used was a twelve-bit ADC with an effective range of 72 dB or ±5 volts. As a result, to maximize the signal-to-noise ratio, an amplifier was needed to boost the signals thereby filling up the required range. It was also necessary on the other hand to ensure that the signal did not saturate in the range or 'clipping' of the signal and thus distortion occurs. Another consideration was that for points on the structure where there was a lot of response, it frequently occurred that after the initial hit, the structure would spring back into the hammer before it could be moved away resulting in a multiple impact. The impacts after the initial hit are typically of such low level at particular frequencies that the signal-to-noise ratio is very much reduced at those points in the frequency spectrum. In order to ensure that the signals properly filled the required range and that multiple impacts had not occurred, the digitized time domain signals were plotted by computer

graphics for viewing. Acceptable signals were then stored on floppy disc for future processing.

3.1.2 Data Processing

Since the time domain data is a limited sample taken from a continuous waveform, the data thus represents the viewing of the continuum through a rectangular window. This corresponds to multiplying the time domain data by a rectangular window function. Multiplication of time domain data by a window function is equivalent to convolution of the Fourier transforms of window and data in the frequency domain. Distortion of the transformed waveforms will thus result unless the time signals are periodic (waveforms form integer multiples of cycles in the finite time period) or decay completely in the time period considered. Added distortion can also occur since random noise in the measurements is not periodic. This distortion is referred to as leakage since signal power 'leaks' out over the frequency spectrum when transformed. Various types of window functions can be used to minimize the leakage depending on the type of waveform examined. Windows also have the effect of reducing the amount of noise in a signal.

The time domain window transformed to the frequency domain assumes the form of a large main lobe followed by a series of smaller side lobes that occur over the rest of the frequency range. Signal distortion is minimized when the main lobe width and side lobes magnitude are minimized. An

unfortunate conflicting property of windows is that by decreasing the main lobe width, the side lobes magnitude increases and there are less noise reduction effects. These properties are proportional to an increasing time domain window width. Thus compromises must be made in choosing the proper window. However, a standard requirement of windows is that to minimize leakage, the window should go to zero at the ends of the time record thereby forcing the signal to be periodic. For example, a common window used on sine waves or random signals is called the Hanning window. This window resembles a Bell curve which tapers to zero at both ends. It can be expressed as a function of the form:

$$w(t) = 0.5\,[1 - \cos(2\pi t/T)] \qquad 0 \leq t \leq T$$

When the impact method is used, windows take on an even greater importance. An important technique used as well in reducing the noise is to take the power spectrum and cross-spectrum of signals at the same points and average them. These are then used to form the frequency response function (to be discussed below). Since the whole point of the impact method is to save time, less averages are taken and thus noise reduction by windowing is very important.

Although the forcing signal for the impact method is self-windowing since it dies out in the time record, stray signals can occur due to hammer movement after the impact. One window which yields reasonable results in this case, is

the squared cosine which drops from unity to zero in 1/16 of the time record. This window can be expressed as:

$$w(t) = \cos^2(8\pi t/T) \qquad 0 \leq t \leq T/16$$

For the case of the response signal in an impact excitation, an exponential window is often used. If the signal decays rapidly, then much of the sampling time period will contain noise. On the other hand, if the structure is lightly damped, then there may be very little decay of the signal and thus there may be no periodicity. This effect will then produce leakage. Both these problems are typically solved by multiplying the response signal by an exponential function which decays exponentially from unity to 0.05 in the time period. Since the important information occurs at the beginning of the time period, it is weighted more heavily. The exponential window is represented as:

$$w(t) = e^{-bt} \qquad 0 \leq t \leq T$$

where:

$$b = \frac{\ln(0.05)}{T}$$

This particular window has the effect of adding additional damping to each mode. However, this damping is a known amount, b. Thus, once the modes have been identified, the damping can be simply subtracted from them to obtain the actual damping. One unfortunate consequence of this window

occurs if the system is already heavily damped. This additional damping may cause the modes to become even more closely coupled and thus harder to identify. In these cases or in general where damping is to be determined more accurately, a Zoom transform can be used. The Zoom transform increases the resolution by concentrating on a narrow frequency band instead of the entire baseband. This technique is discussed in Ramsey [21] and was not used in the present study.

It is important to note that with both the forcing and response windows, there was no need to force a zero amplitude at the beginning of the time period. Both are inherently zero as the structure has not yet been excited.

The determination of the frequency response function (FRF) can be determined from its basic definition:

$$H = \frac{S_r}{S_f}$$

However, to reduce the inherent noise effects, it is actually done by using averages of power and cross-spectrums. To understand how this is done, consider the response spectrum as:

$$S_r = HS_f + S_n$$

where S_n is the noise Fourier spectrum. While the effect of the noise can be substantially reduced by averaging the

spectrums, since they are complex, they do not readily lend themselves to this averaging process. It is easier to use the power spectrums which for the response and forcing are defined respectively as:

$$G_{rr} = S_r S_r^* \qquad G_{ff} = S_f S_f^*$$

Taking the square root of the ratio of the above quantities would yield the FRF. However, in this form there is no phase information and the noise will not average out. The cross-power spectrum can be used for this purpose. It can be defined as:

$$G_{rf} = S_r S_f^*$$

and thus the FRF can be defined as:

$$H = \frac{S_r}{S_f} \cdot \frac{S_f^*}{S_f^*} = \frac{G_{rf}}{G_{ff}}$$

Averaging in the presence of noise yields:

$$\overline{G_{rf}} = \overline{S_r S_f^*} = \overline{(S_f H + S_n) S_f^*} = \overline{G_{ff} H} + \overline{G_{nf}}$$

and thus:

$$H = \frac{\overline{G_{rf}}}{\overline{G_{ff}}} - \frac{\overline{G_{nf}}}{\overline{G_{ff}}}$$

where the second term numerator is the noise cross-power spectrum. Since the noise and forcing signals are uncorrelated, the noise cross-power spectrum will average to zero and thus a closer approximation to the true FRF can be determined.

In order to quantify the amount of noise in a FRF measurement, the coherence function is computed. This coherence function can be defined as the ratio of the response power caused by the applied force to the measured response power.The measured response power can be expressed as:

$$G_{rr} = S_r S_r^* = (HS_f + S_n)(HS_f + S_n)^*$$

$$= | HS_f |^2 + H^* S_n S_f^* + HS_f S_n^* + S_n S_n^*$$

$$= | H |^2 G_{ff} + H^* G_{nf} + HG_{fn} + G_{nn}$$

Averaging will thus yield:

$$\overline{G_{rr}} = | H |^2 \overline{G_{ff}} + \overline{G_{nn}}$$

The response power caused by the applied force is:

$$(HS_f)(HS_f)^* = | H |^2 G_{ff} = \frac{G_{rf} G_{rf}^*}{G_{ff}} = \frac{| G_{rf} |^2}{G_{ff}}$$

where averaging will give:

$$|H|^2 \overline{G_{ff}} = \frac{|\overline{G_{rf}}|^2}{\overline{G_{ff}}}$$

Therefore, the coherence can be expressed as:

$$\gamma^2 = \frac{|H|^2 \overline{G_{ff}}}{|H|^2 \overline{G_{ff}} + \overline{G_{nn}}} = \frac{|G_{rf}|^2}{\overline{G_{ff}}\,\overline{G_{rr}}}$$

As a result, if the coherence is one, then the response is due solely to the forcing and thus no noise is present. All values of less than one suggest noise contamination quantified by the particular value.

3.2 Modal Parameter Estimation

Once the FRF's have been formed, accurate estimation of the modal parameters is done by curve fitting. Each FRF formed at each point on the structure represents the sum of the contribution of each mode in the frequency range of interest. If there is a large amount of frequency separation and little modal damping, then the effect of one mode on another is minimal and a curve fit that fits one mode at a time is adequate. The assumption then is that each mode can be represented by a single degree-of-freedom model. However, often the situation is such that the modes have a marked effect on one another and there is thus strong modal coupling. In this situation, the modal parameters must be identified simultaneously. Single mode and multiple mode

methods are discussed in some detail in Richardson [24]. A very good multiple mode curve fitting algorithm is described in some detail in Richardson and Formenti [25]. The method used in this study for modal parameter estimation was an algorithm developed by Fyfe [7] based on a complex curve fitting scheme devised by Levy [15]. This method curve fits the experimental data to the analytical function as formulated in equation (2.5) for $s = j\omega$. The fit is a multiple mode one in which minimization of error uses a least squares technique. This method is thoroughly discussed in the reference by Fyfe.

It should be noted that usually modal analysis revolves around the use of specialized equipment such as the Fourier analyzer to collect and process the data. For advanced analysis like multiple mode curve fitting, a computer is also required. This study bypassed the Fourier analyzer and used a complete mini-computer software package developed by Fyfe to collect, process and curve fit the data.

3.3 Calibration

The traditional technique of calibration involved the determination of the individual sensitivites of the accelerometer and load cell by comparison with a standard. This method, however, has several problems associated with it. These include inconvenient on-site calibration, accumulation of errors due to individual calibration and the fact that amplitude is usually measured at only a few

frequencies with phase being entirely ignored. In addition, there is typically a lack of regard for auxillary equipment such as amplifiers and filters.

For the impact technique, the traditional calibration can lead to entirely erroneous results. The force picked up by the load cell is not equal to the force exerted on the structure due to an effective mass between the load cell and the structure. This effective mass being due to the impact tip mass and its material properties. Another technique which circumvents many of these problems is called ratio calibration. The combination of hammer, load cell, impact tip and accelerometer used to measure the dynamics of the structure considered can be calibrated simultaneously. This task is accomplished using a very simple experimental set-up.

A relatively large block of known mass is hung from a long suspension. This set-up can be made to approach a single degree-of-freedom system if the suspension is long enough and if there is little motion through the block's center of gravity. Thus by mounting an accelerometer on one end of the block and impacting it through its center of gravity at the opposite end, the force can be expressed through Newton's law as:

$$F = m_c A$$

or

$$\frac{A}{F} = \frac{1}{m_c}$$

This relation thus represents the inertance or expected FRF of the calibration block and is a constant (inverse of the block mass). A calibration function can be defined then as the ratio of the expected FRF to the measured FRF expressed as:

$$H_C = \frac{1/m_C}{A_I/F_I} = \frac{1}{m_C H_I}$$

where:

H_C - calibration function
H_I - measured FRF of calibration block
m_C - mass of calibration block

Assuming linearity for an actual structure being tested, its measured FRF can be calibrated by multiplying it by the calibration function to obtain the actual FRF. This relationship can be simply shown as:

$$H_A = H_C H_M$$

The actual FRF will be in physical inertance units depending on the physical units used for the calibration block. To convert to compliance units, it is only necessary to divide through by $(j\omega)^2$.

3.4 Structural Dynamics Modification

Structures whose mode(s) possess proportional or very light damping can usually be described in terms of a real or normal mode model. At a particular mode, this model is characterized by a mode shape which attains maximum or minimum deflections simultaneously. As a result, different points on the structure are either in phase or 180° out of phase and thus nodal points are stationary. In actuality, all structures possess damping where the modes are complex to some degree. This implies that a mode shape will not reach maximums or minimums simultaneously and thus nodal points 'travel' i.e. the phases will assume values other than 0° or 180°.

However, since a majority of the mechanical structures dealt with possess relatively little damping, it is not very often when truly complex modes are encountered. Even when they are, they are almost impossible to adequately identify as such due to practical measurement problems. These include the inherent problems of noise, transducer and instrumentation phase match characteristics, leakage and errors in parameter estimation. Formenti and Welaratna [6] examined several of these problems and their effects using simulation. They have found through experience that the errors in assuming a real mode model are much less than those occurring when trying to estimate complex modes. As a result, the SDM technique utilizes a real mode model. Damping is taken into account through the assumption of

proportionality as shown in section 2.2.

The curve fitter in this study (section 3.2) results in complex frequencies and mode shapes. Therefore, the mode shapes can be approximated as real by considering only the magnitude of the residues and determining their sign by rounding off the phase. Because of the assumption of proportional damping, the complex frequencies can be retained as complex. When the modal parameters have been converted, a real mode model with proportional damping can be constructed.

Once the physical modification value and location are decided and the mode shapes have been normalized to unit modal mass, then the modified systems damping and natural frequencies or complex eigenvalues (Ω) can be calculated from equation (2.23). Rearranged in terms of a function, it becomes:

$$F(\Omega) = \left[\sum_{k=1}^{n} \frac{\phi_k^2}{(\Omega^2 + 2\sigma_k\Omega + (\sigma_k^2 + \omega_k^2))} \right] + \frac{1}{(\alpha\Omega^2 + \beta\Omega + \gamma)}$$

where:

$$\{\phi\} = [\Phi]^T\{1\}$$

Thus at a point on the structure where there is a mass modification and/or stiffness and damping changes applied to ground, the vector $\{\phi\}$ is the row of the modal matrix $[\Phi]$ corresponding to that particular point or DOF. For damping and stiffness applied between two points or DOF's, the vector $\{\phi\}$ is the difference between the two corresponding

rows in the modal matrix.

Equation (2.23) represents the modified systems characteristic equation. It is possible to expand equation (2.23) into a characteristic polynomial. The solution could then be accomplished using any of the numerous polynomial algorithms available. However, for systems greater than 1 DOF, the expansion into the polynomial becomes an increasingly difficult task. Fortunately, the roots can still be found from the original form by using the Newton-Raphson method. This method is iterative where the iterative equation is formulated as:

$$\Omega^{r+1} = \Omega^{r} - \frac{F(\Omega^{r})}{F'(\Omega^{r})}$$

where 'r' denotes the iteration and F' is the functional derivative of equation (2.23) expressed as:

$$F'(\Omega) = \frac{dF}{d\Omega} = \left[\sum_{k=1}^{n} \frac{-2\phi_k^{\,2}\,(\Omega + \sigma_k)}{(\Omega^2 + 2\sigma_k\Omega + (\sigma_k^{\,2} + \omega_k^{\,2}))^2}\right] - \frac{(2\alpha\Omega + \beta)}{(\alpha\Omega^2 + \beta\Omega + \gamma)^2}$$

Once the complex frequencies have been determined, it is a straight forward process to obtain the eigenvectors or mode shapes by direct substitution into equation (2.24). Transformation of the modified mode shapes back to physical coordinates is then accomplished by using equation (2.13).

The Newton-Raphson method was both easy to program and converged to complex frequencies rapidly. However, for very small values of ϕ_k (little modal motion) or relative

modification values, it was found that convergence to a modified structure frequency did not occur. As a result, it was deemed a valid assumption that the modal frequency was not affected and thus the previous unmodified value was retained.

Initially the Newton-Raphson method was coupled with the Incremental-Search method so as to make the root finding process automatic. It was found to be much faster however, to simply use an interactive approach whereby initial values were manually input.

4. RESULTS AND DISCUSSION

In the previous chapters, the theoretical and practical aspects of EMA and SDM have been individually examined. This chapter follows the next logical steps of first separately verifying these techniques through an example of a well known structure (a free-free beam) and then evaluating the combination of the two techniques by application to a more complex structure.

4.1 Calibrated EMA Validation

As a check on the modal analysis technique, a free-free beam was experimentally tested and the calibrated results obtained were compared to theoretical results. The calibration procedure followed that as outlined in section 3.3. The calibration mass used was an arbitrary block of steel with dimensions 2 in x 2 in x 5 in (50.8 mm x 50.8 mm x 127 mm) resulting in a mass of 0.0146 lb-sec^2/in (2.55 kg). Initial theoretical calculations for the free-free beam placed the first three modes at just under 1000 Hz and as a result, the calibration FRF was determined with a cut-off at 1000 Hz. It is important to note that since two FRF's were multiplied together (section 3.3), they must have compatible frequency resolutions.

The experimental set-up for the free-free beam consisted of a steel beam with dimensions 3/8 in x 3/2 in x 22 in (9.53 mm x 38.1 mm x 559 mm) suspended by elastic bands. Eleven equal locations from one end to the other were

marked off and tested for lateral vibration up to 1000 Hz. The same accelerometer as that used in calibration was mounted at the first point at the end of the beam in the vertical direction and the same hammer was used to impact the beam at all eleven locations.

The first test point coherence and calibrated inertance FRF is shown in figure 4.1. The entire plot actually consists of the three separate plots of coherence and the FRF magnitude and phase. The dashed line corresponds to the curve fit results. It can be seen from the figure that there are three well defined modes with very little damping. Since the coherence is essentially unity at all three peaks and the curve fit conforms to them very well, this measurement should be expected to accurately portray the dynamics at this point. Table 4.1 shows the excellent agreement between the experimental (averaged over all the test points) and theoretical frequencies.

Since SDM uses mode shapes normalized to unit modal mass (section 2.2), and since this directly corresponds to the degree of modal participation as well as calibration and EMA accuracy, both the calibrated test and theoretical mode shapes were compared in this form as shown in table 4.2. The table shows that the first and second mode shapes are very close to their theoretical counterparts while the third mode shape is not as good. It was found that in most of the measurements, the coherence was not as good in the vicinity of the third mode. This fact is especially evident at test

MODE	DAMPING (%) THEORY	DAMPING (%) TEST	FREQUENCY (Hz) THEORY	FREQUENCY (Hz) TEST
1	0.0	0.06	158.5	159.4
2	0.0	0.06	436.8	438.8
3	0.0	0.04	856.3	858.8

Table 4.1 Comparison Between Theoretical and Experimental Frequencies for the Free-Free Beam

TEST POINT	MODE 1 THEORY	MODE 1 TEST	MODE 2 THEORY	MODE 2 TEST	MODE 3 THEORY	MODE 3 TEST
1	21.2	22.2	21.2	22.1	21.2	22.2
2	11.4	11.1	4.8	4.6	-11.0	- 1.7
3	2.1	2.3	- 8.4	- 8.1	-13.5	-15.8
4	- 5.8	- 5.6	-14.0	-13.7	- 8.4	- 8.0
5	-11.0	-10.8	-10.2	-10.3	6.9	7.3
6	-12.9	-12.6	0.0	0.3	15.1	18.2
7	-11.0	-10.7	10.2	10.2	6.9	8.7
8	- 5.8	- 5.5	14.0	13.7	- 8.4	-10.8
9	2.1	2.2	8.4	8.1	-13.5	-16.0
10	11.4	11.1	- 4.8	- 4.7	-11.0	- 1.6
11	21.2	21.9	-21.2	-21.6	21.2	20.2

Table 4.2 Comparison Between Theoretical and Experimental Mode Shapes for the Free-Free Beam

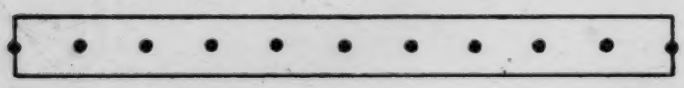

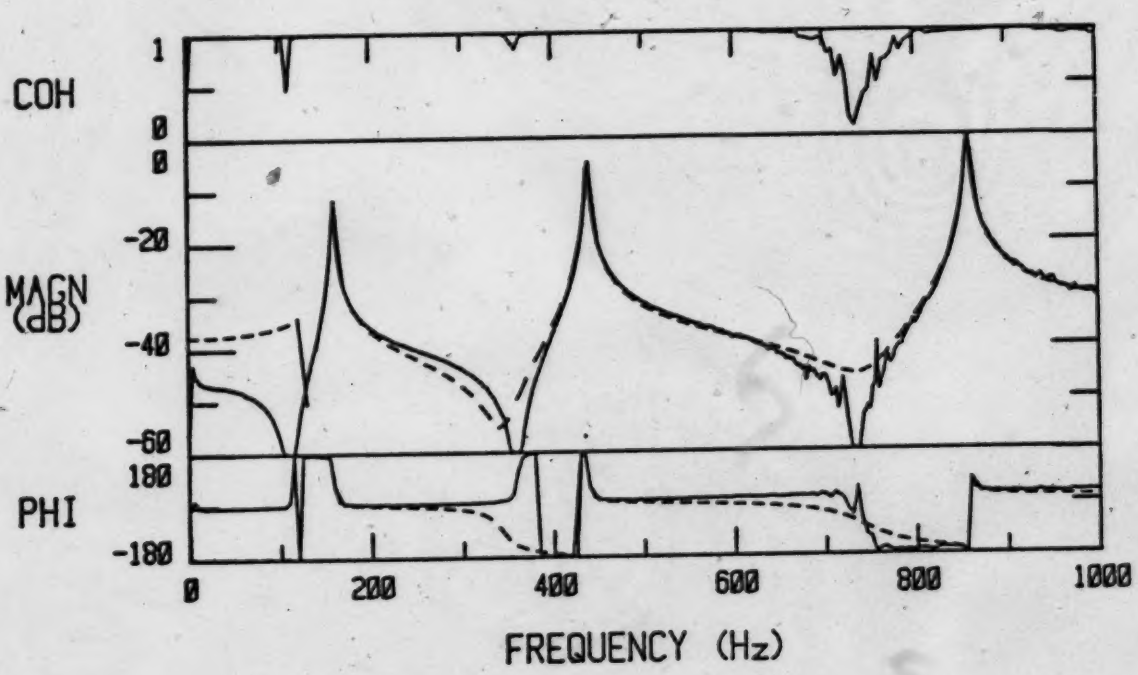

Figure 4.1 FRF and Coherence for the Free-Free Beam at Test Point 1

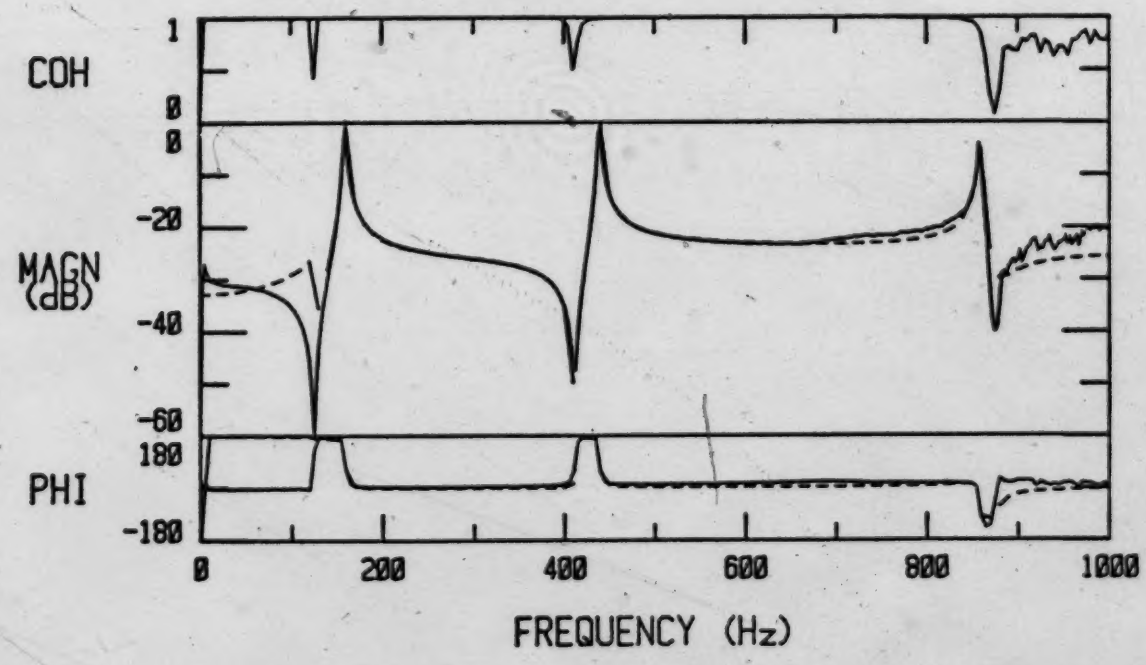

Figure 4.2 FRF and Coherence for the Free-Free Beam at Test Point 2

point 2 which gave the poorest mode shape estimate. The coherence and FRF for test point 2 is shown in figure 4.2. It is evident that while the EMA technique and calibration can be quite accurate, noise can greatly affect this accuracy as evidenced by the coherence in figure 4.2.

4.2 SDM Validation

In order to check the accuracy of the SDM method, the theoretical modal parameters for the free-free beam described in the previous section, were used as input to the SDM program. The theoretical modal model used was described by six modes including the two rigid body modes. This model is shown in tables 4.3 and 4.4 where the mode shapes have again been normalized to unit modal mass. This model was modified using SDM and compared to the corresponding theoretical solution. The modifications consisted of the separate addition of a pin, a stiffness of 10,000 lb/in ($1.75(10^6)$ N/m) and a mass of 1 lb (0.454 kg) to point 1. The pinned modification was modelled in the SDM technique by adding an infinite stiffness. This simply results in the left hand side of equation (2.23) going to zero. Table 4.5 represents the theoretical non-rigid body frequencies in comparison to the predicted using a varying number of input modes for the three separate modifications. In each case, the relative modification was large in order to adequately test SDM accuracy. As was expected, the accuracy diminishes for predictions at higher modes (since the model is

MODE	FREQUENCY (Hz)
1	0.0
2	0.0
3	158.5
4	436.8
5	856.3
6	1415.6

Table 4.3 Theoretical Free-Free Beam Frequencies

POINT	MODE 1	MODE 2	MODE 3	MODE 4	MODE 5	MODE 6
1	10.6	-18.4	21.2	21.2	21.2	21.2
2	10.6	-14.7	11.4	4.8	-11.0	- 6.2
3	10.6	-11.0	2.1	- 8.4	-13.5	-12.7
4	10.6	- 7.4	- 5.8	-14.0	- 8.4	4.8
5	10.6	- 3.7	-11.0	-10.2	6.9	14.8
6	10.6	0.0	-12.9	0.0	15.1	0.0
7	10.6	3.7	-11.0	10.2	6.9	-14.8
8	10.6	7.4	- 5.8	14.0	- 8.4	- 4.8
9	10.6	11.0	2.1	8.4	-13.5	12.7
10	10.6	14.7	11.4	- 4.8	-11.0	6.2
11	10.6	18.4	21.2	-21.2	21.2	-21.2

Table 4.4 Theoretical Free-Free Beam Mode Shapes

	PIN ADDITION				STIFFNESS ADDITION				MASS ADDITION			
MODE	THEORY	SDM (6)	SDM (5)	SDM (4)	THEORY	SDM (6)	SDM (5)	SDM (4)	THEORY	SDM (6)	SDM (5)	SDM (4)
1	109.2	109.5	109.7	110.2	106.1	106.4	106.5	107.0	126.2	126.3	126.4	126.7
2	353.9	355.9	357.7	363.2	319.9	322.1	324.2	330.6	372.6	374.4	375.7	379.4
3	738.4	747.0	756.4		587.2	594.7	603.2		759.0	765.5	772.6	
4	1262.7	1290.8			941.2	948.4			1284.1	1306.6		

Table 4.5 Summary of Predictions of Modifications to the Free-Free Beam (Hz)

truncated) or if fewer modes were used in the prediction. However, it is important to note that the accuracy did not diminish exponentially but much more gradually.

To determine mode shape prediction accuracy as well, a fourth change was made. The full six mode free-free beam model was used to predict the effect of two local modifications which pinned both ends of the beam. The comparison in terms of both frequency and mode shape (normalized to unit modal mass) with the theoretical is shown in tables 4.6 and 4.7. It can be seen that the prediction is quite good overall, but accuracy again diminishes for higher frequencies.

4.3 Unmodified Test Structure

The structure chosen to be tested was built to be similiar to that used by Herbert and Kientzy [11] and Ramsey and Firmin [23]. A schematic diagram of this structure is given in figure 4.3. It consists of three aluminum plates bolted together along the adjoining edges. In order to determine the mode shapes accurately, a grid comprised of seventeen test points was established on the top plate. No points were used for the back plate since the motion could be deduced from top plate information. Only two points were deemed necessary for the bottom plate since it was large and heavy relative to the other two and thus little response was expected. The total number of test points then was nineteen, each with 3 DOF (x,y and z directions) resulting in a total

MODE	FREQUENCY (Hz) THEORY	SDM
1	69.9	70.3
2	279.6	281.8
3	629.1	645.7
4	1118.5	1147.7

Table 4.6 Theoretical and Predicted Frequencies for the Pinned-Pinned Configuration

TEST POINT	MODE 1 THEORY	SDM	MODE 2 THEORY	SDM	MODE 3 THEORY	SDM	MODE 4 THEORY	SDM
1	0.0	0.0	0.0	0.0	0.0	0.0	0.0	0.0
2	4.6	4.7	8.8	8.6	12.1	18.2	14.3	12.7
3	8.8	8.8	14.3	14.3	14.3	14.3	8.8	9.8
4	12.1	12.2	14.3	14.3	4.6	5.7	- 8.8	- 8.0
5	14.3	14.3	8.8	8.7	- 8.8	- 8.8	-14.3	-15.4
6	15.0	15.0	0.0	0.0	-15.0	-16.0	0.0	0.1
7	14.3	14.2	- 8.8	- 8.8	- 8.8	- 8.8	14.3	15.4
8	12.1	12.2	-14.3	-14.4	4.6	5.8	8.8	8.0
9	8.8	8.8	-14.3	-14.3	14.3	14.3	- 8.8	- 9.9
10	4.6	4.6	- 8.8	- 8.6	12.1	18.1	-14.3	-12.7
11	0.0	0.0	0.0	0.0	0.0	0.0	0.0	0.0

Table 4.7 Theoretical and Predicted Mode Shapes for the Pinned-Pinned Configuration

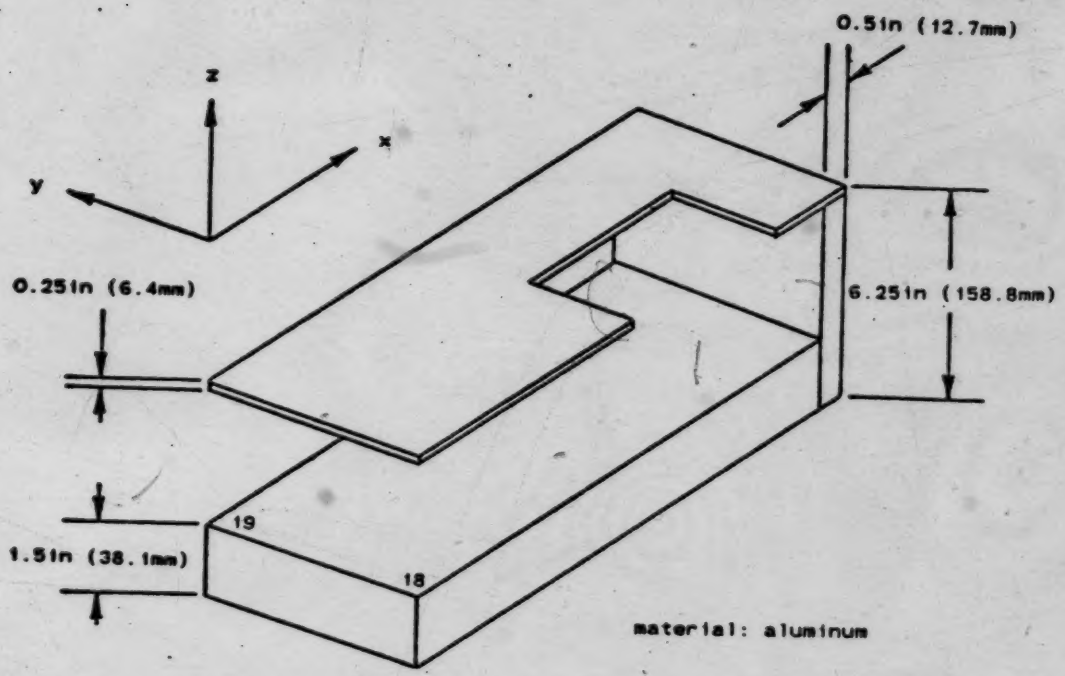

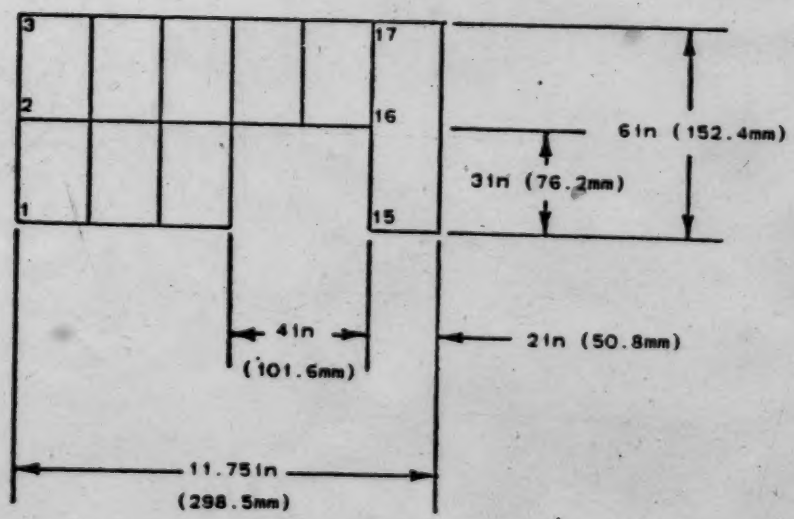

Figure 4.3 Original Test Structure

of 57. Since many of the points were internal to the structure, this total was reduced to 30. In order to simulate a free-free condition, the structure was placed on a block of foam rubber for all measurements.

As before, the modal information was obtained using the impact method with an accelerometer fixed in the z direction at point 1 (thus point 1z). Preliminary tests displayed the existence of five distinct vibrational modes under 400 Hz. Therefore, with a sampling frequency of 1024 Hz, the frequency resolution was a very acceptable 1 Hz. It was possible to impact the structure at all points in the perpendicular or z direction. To obtain information in the plane of the structure (x and y directions), selected points were impacted parallel to the surface. Since the accelerometer was fixed at point 1z, and impacted at all others, the first row of the transfer function matrix was measured.

The FRF information which was curve fitted for point 1z up to 400 Hz (figure 4.4) shows the five distinct vibrational modes as well as the occurrence of two rigid body modes at the lower end of the frequency scale. The coherence at this point and for most of the others in the z direction were very good. It was however, typically much poorer for measurements in the x and y directions. This effect can most likely be attributed to low response levels (and thus lower signal-to-noise ratios) in those directions and perhaps transverse sensitivity effects of the

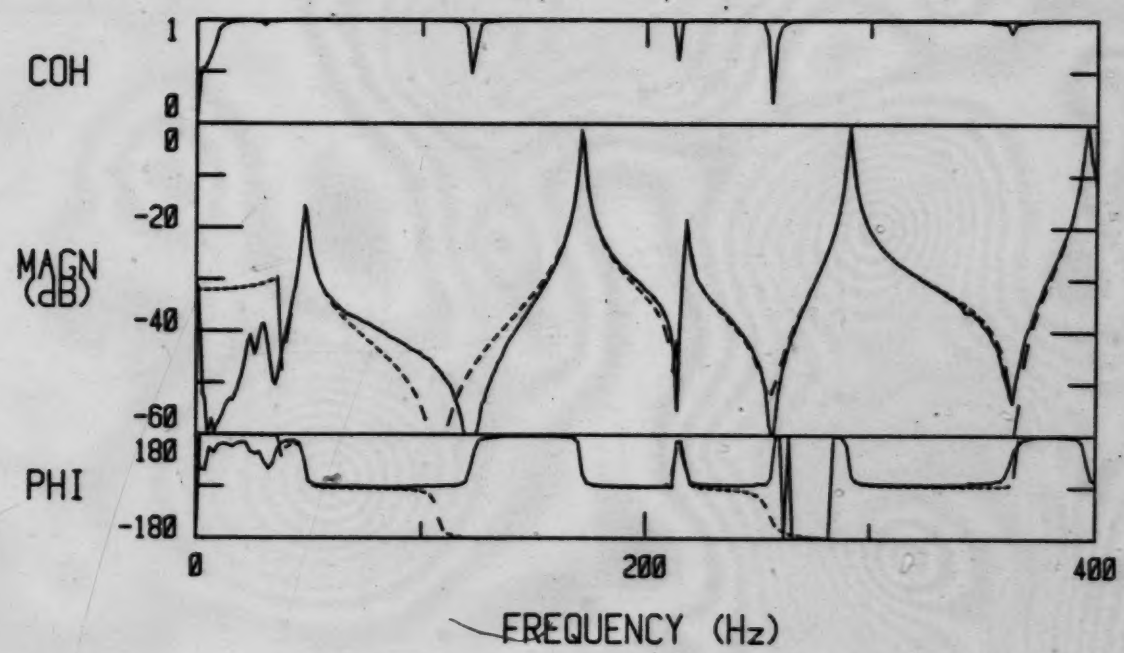

Figure 4.4 FRF and Coherence for the Original Structure at Test Point 1z

accelerometer.

The modal parameters obtained in the z direction are shown in tables 4.9-4.14 where the mode shapes were again normalized to unit modal mass. Since damping and natural frequency are global properties of a structure they have been averaged and presented as shown. The geometrical representation of the mode shapes for the five modes are shown in figure 4.5. The first mode at 48.2 Hz represents an almost purely flapping mode of the top plate (first bending) whereas the second mode at 171.3 Hz displays almost pure torsion of the top plate around the x axis (first torsion). The third at 217.9 Hz is comprised of a combination of top plate torsion around the x axis and back plate torsion or twisting around the z axis. The fourth and fifth modes at 290.8 Hz and 395.8 Hz respectively, are essentially 'rippling' modes of the top plate (second bending in and out of phase).

An examination of the mode shapes indicates that point 3 undergoes relatively large excursions in the first three modes. As a result, this point was chosen for modifications as it appears that this would cause large dynamic changes and thereby give a thorough test of the SDM concept.

4.4 Effects of Mass Modification

The simplest modification to implement consisted of an addition of 0.25 lb (mass of 0.11 kg) of lead at point 3. This configuration was tested using EMA at the same test

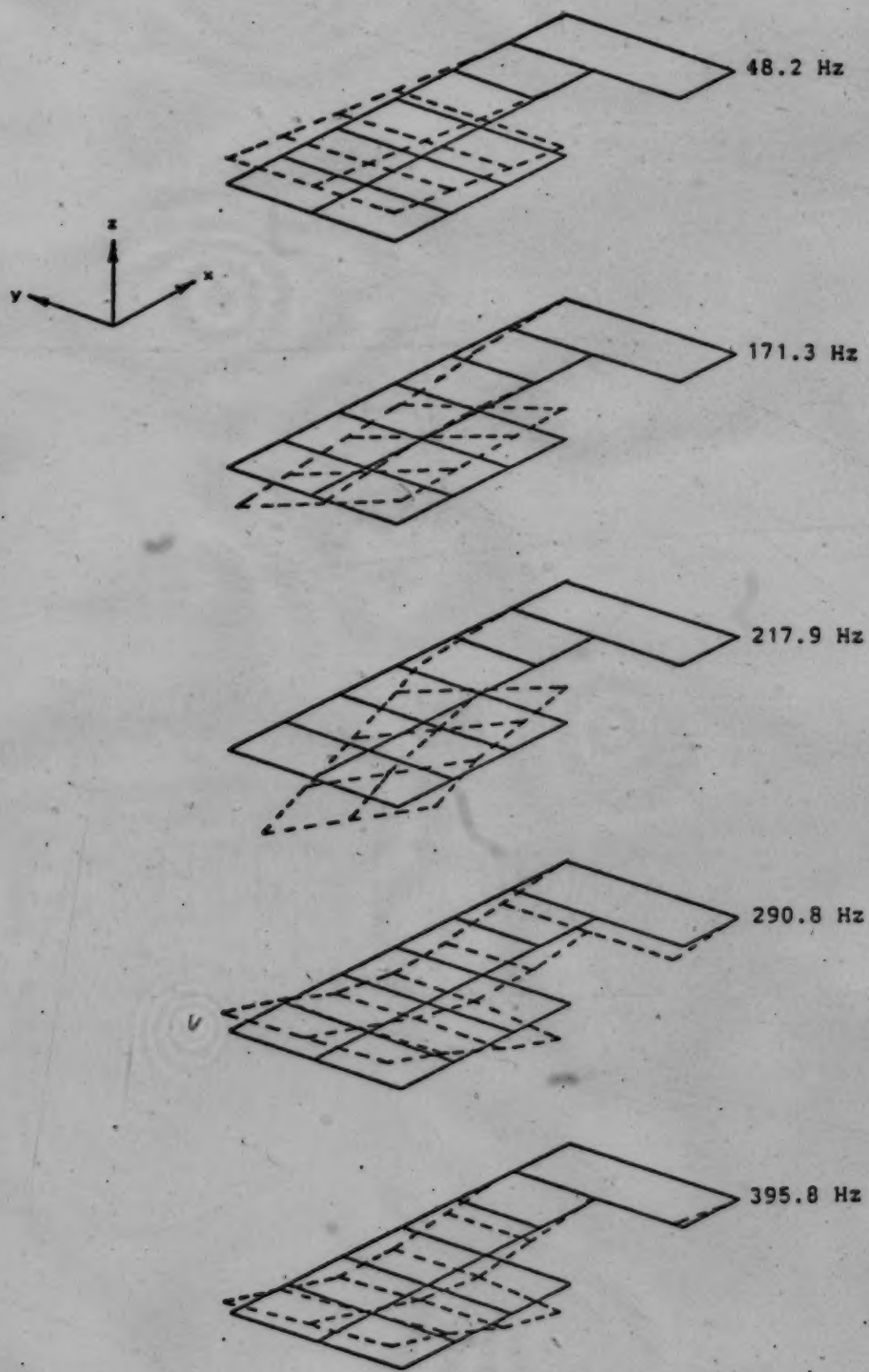

Figure 4.5 Original Test Structure Mode Shapes

points as in the original structure. The FRF, curve fit and coherence are shown again for point 1z in figure 4.6. The most obvious effect of the mass was an overall reduction of the natural frequencies.

In order to model this change using SDM, the mass was added to all 3 DOF (x,y and z directions) at point 3 so that in affect three local modifications were performed. The modal frequency comparison between the test and the predicted results are shown in table 4.9. The predicted effect on the mode shapes in the z direction is summarized in tables 4.10-4.14. It can be seen from table 4.9 that the prediction is good when considering the magnitude of the changes in frequency. The second and third mode frequencies show the greatest discrepancies most likely due to a combination of several factors. The first factor relates to the fact that these modes had the largest contributions from all three directions with the result that the motion is more complex and thus more dependent on three measurements instead of one. Secondly, the measurements in the x and y directions were more prone to noise effects as explained above and thus poorer estimates of modal parameters were used in the prediction. The last factor, which is probably the most important, is that rotational inertia of the mass is not taken into account. Complete motion at a point involves not only the translational motion in the x,y and z directions but also rotations around each axis. Thus, to accurately predict the motion, rotational DOF's should be

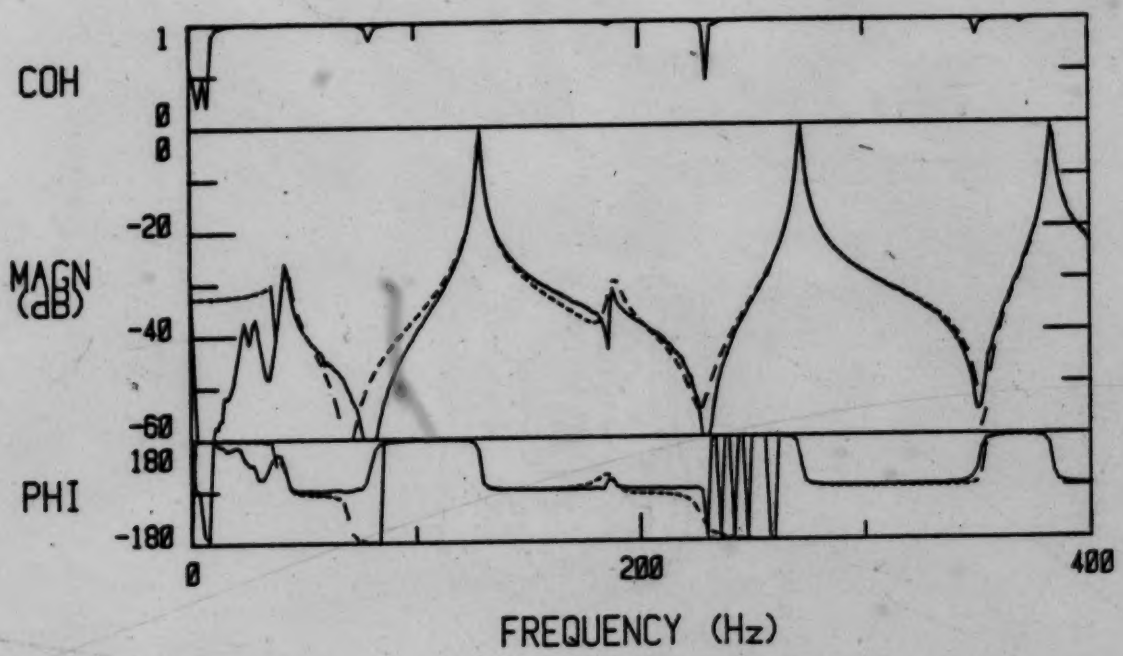

Figure 4.6 FRF and Coherence for the Mass Modified Structure at Test Point 1z

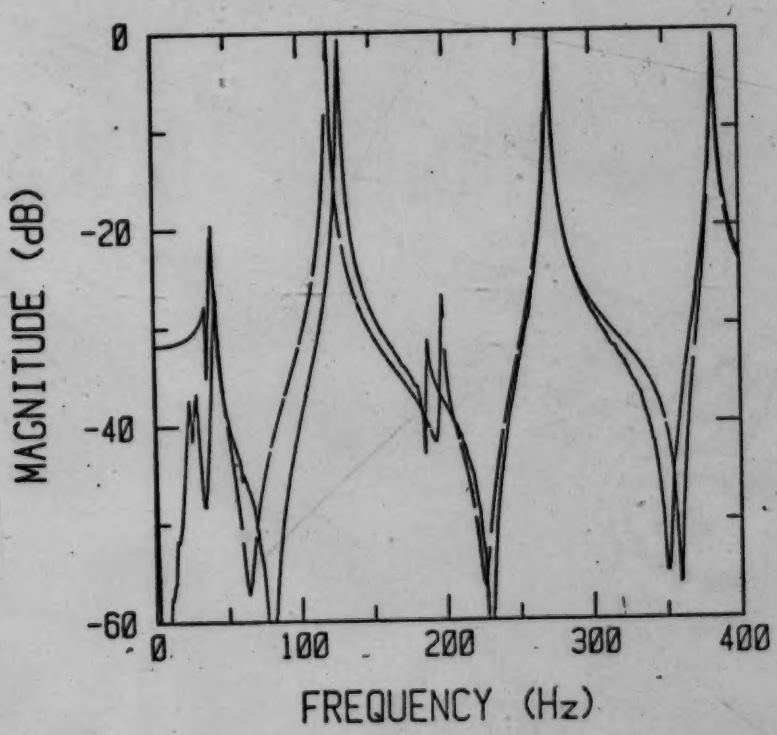

Figure 4.7 Mass Modified Structure Synthesis Plot

added. This is especially important for beam structures, such as the test structure considered here, where rotational effects are most pronounced. Unfortunately, rotations are difficult to measure and thus there are no commercially available transducers. However, rotations can be estimated using several translational transducers. Discussion of rotational DOF and their estimation has been done in references [2] and [29].

A more complete way of displaying the entire prediction in terms of frequencies and mode shapes is to synthesize an element of the modified FRF matrix and compare it to the actual FRF measured. This synthesis is in the form of a plot of the magnitude for point 1z and is shown in figure 4.7 for the mass change. The solid line represents the magnitude of the measured FRF and the dashed line displays the predicted. As is seen, the magnitudes are also quite close which implies an accurate prediction for the mode shape as well. Again, the largest deviations appear to occur at the second and third modes due to the reasons previously discussed.

4.5 Effects of Stiffness Modification

The second type of change considered was the addition of stiffness. Once again, in order to provide large relative changes in the test results, the change included attachment at point 3. A brass rod 1/16in (1.6mm) in diameter was attached between points 3 and 19. Using simple beam theory and assuming built-in end conditions, the stiffness in all

three directions was calculated from:

$$k_z = \frac{AE}{L} \qquad k_x = k_y = \frac{3EI}{L^3}$$

where A is the cross-sectional area, L is the length, I is the area moment of inertia and E is the Young's modulus. This rod gave calculated values of k_z of 10,500 lb/in ($1.84(10^6)$ N/m) and k_x and k_y of 0.4 lb/in (70 N/m). The total weight of the stiffening rod addition was 0.016 lb (mass of 0.0073 kg) and this was evenly divided between points 3 and 19. The FRF, curve fit and coherence for the stiffness addition for point 1z is shown in figure 4.8. The main effect of the stiffness was to raise the natural frequencies so that only four modes occurred in the frequency range of interest. As seen in table 4.9, the lowest mode occurred at approximately 106 Hz whereas in the original structure it was at 48 Hz.

To model the change using SDM, the stiffnesses were added in the respective directions between the two points and also half the total mass was added to each of the points 3 and 19. However, it was found that the small amount of mass and the x and y stiffnesses caused negligible changes in the structure's dynamics. The longitudinal or z direction stiffness though, resulted in large changes in frequency as shown in table 4.9. The changes in the mode shapes can again be seen in tables 4.10-4.14. The tested and predicted results from table 4.9 agree very well. This good agreement

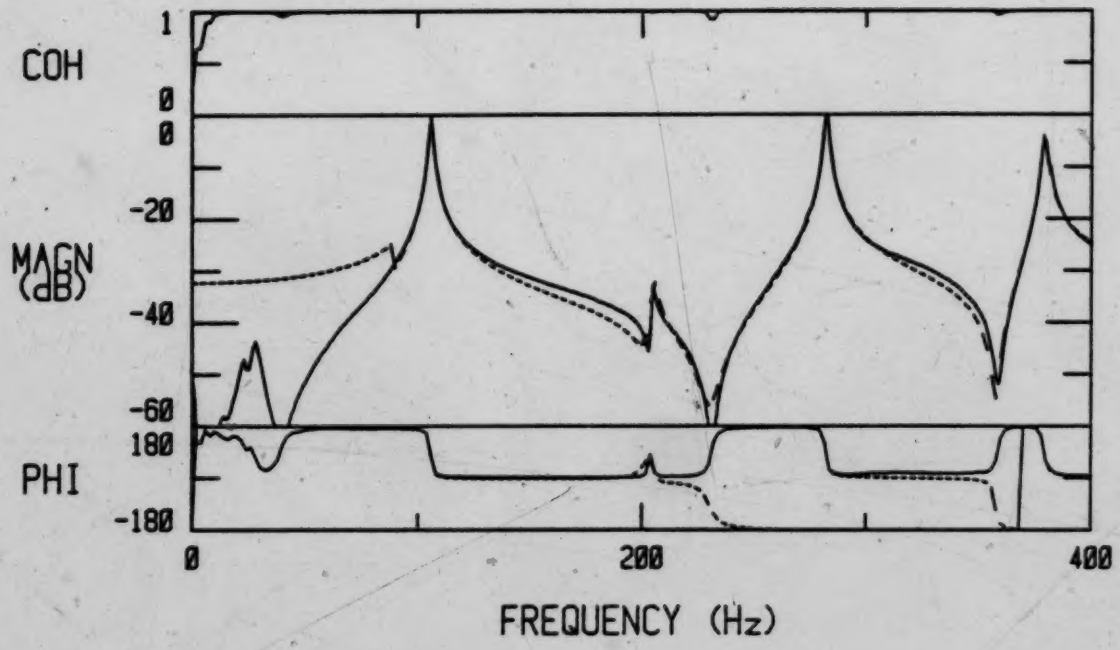

Figure 4.8 FRF and Coherence for the Stiffness Modified Structure at Test Point 1z

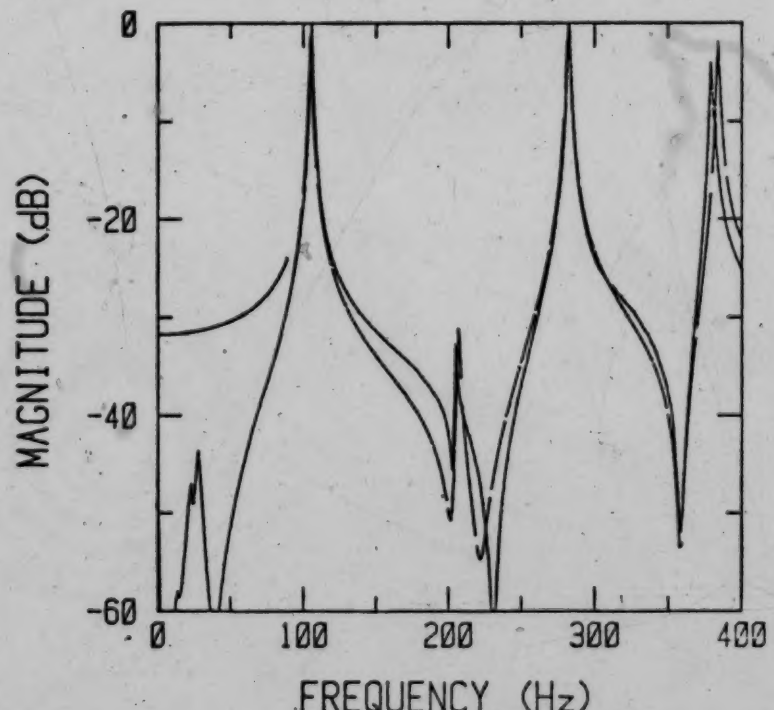

Figure 4.9 Stiffness Modified Structure Synthesis Plot

is due to the fact that essentially only one local modification was needed, that rotational DOF's could be safely ignored and that very good original modal parameters (z direction only) were used in the prediction. The synthesis plot for the stiffness change is presented in figure 4.9 for point 1z. The mode shape can be seen to be very close as well.

It should be noted that since five modes were utilized in the modal model, that a fifth mode was also predicted. It was found that the predicted fifth mode occurred at 1019 Hz. Although the actual structure was not tested for the fifth mode (it exists outside the frequency range of interest), it seems highly unlikely that the fifth mode would jump from 395.8 Hz to over 1000 Hz. The explanation for this behavior is that the modal model used is a truncated one which was built around information only from DC to 400 Hz. Therefore, it would not be expected to predict the dynamic effects very far outside the scope of this model.

Comparable results for similiar mass and stiffness modifications to a similiar structure can be found in references [11] and [23].

4.6 Effects of Damping Modification

The final modification considered was the introduction of increased damping. This change was expected to yield the least predictable results for a variety of reasons. These include the fact that proportional linear viscous damping is

assumed and also that a real mode model is being used to model a complex mode phenomena. As well, it is known that material properties such as shear modulus and damping coefficient are quite dependent on frequency, temperature, dynamic load and static preload.

The physical modification consisted of a damper designed in the form of an annular rubber shear mount. A diagram of the damper is shown in figure 4.10 and is comprised of a brass casing filled with a soft prosthetic rubber of about 20 durometer hardness. A brass plunger was then cemented into the rubber in the center of the mount. An end of rod soldered to the casing was then screwed into the structure at point 19 while the opposite end of the plunger was screwed in at point 3. The design was based on the formulation for stiffness given by Macduff and Curreri [16] for rubber shear mounts. It was desired to minimize the amount of stiffness, considering physical constraints, and to accentuate the damping contribution. The longitudinal stiffness for annular rubber shear mounts is approximated as:

$$k = \frac{2\pi LG}{\ln\left(\frac{r_o}{r_i}\right)}$$

where L is the length, r_o and r_i are the outside and inside radii respectively and G is the shear modulus for the rubber.

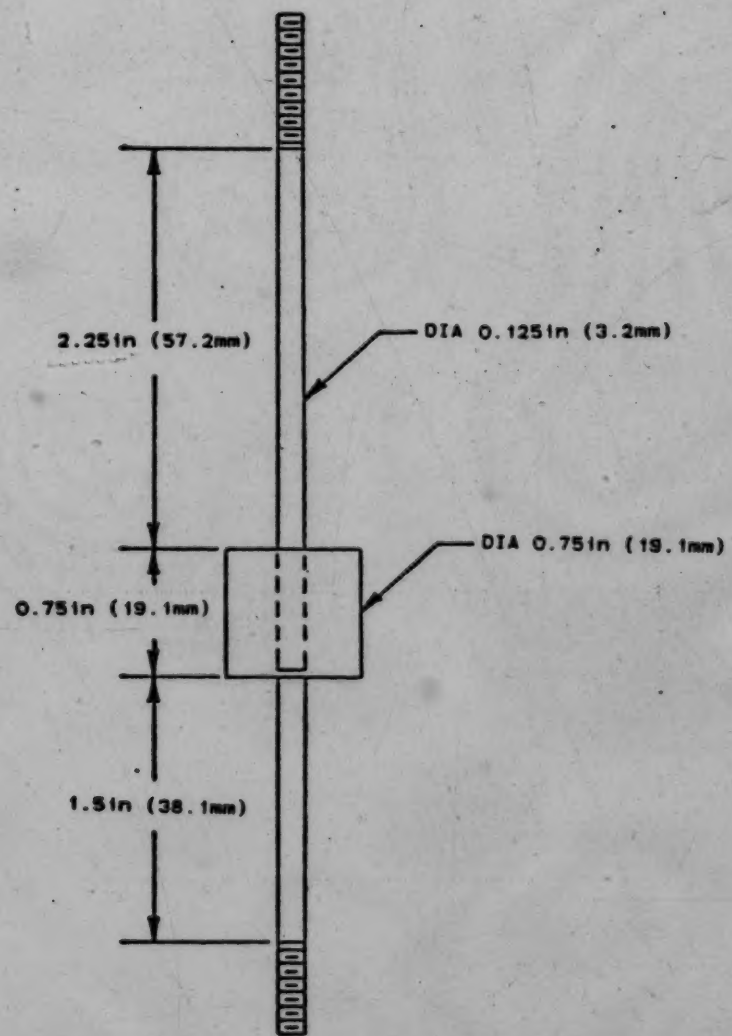

Figure 4.10 Annular Rubber Shear Mount Damper

A more accurate determination of the stiffness and damping was accomplished by testing the rod-rubber combination. This configuration was fixed with one end on a shaker table and a mass attached to the other end so as to approximate an oscillating support problem for a damped single DOF system. Accelerometers attached at the mass and the shaker ends allowed determination of the maximum ratio between the amplitude at the mass (X) and the amplitude at the shaker (Y) which for a linear viscous system forms the relation:

$$\left(\frac{x}{y}\right)_{max} = \frac{\sqrt{(m\omega_f)^2 + c^2}}{c}$$

where m is the mass on the end resonating at the input forcing frequency and c is the single unknown, the viscous damping constant. The stiffness of the rod is then calculated from:

$$k = m\omega_f^2$$

The mass was selected so as to obtain a forcing frequency approximately midway in the frequency range of interest. The damping constant and stiffness were thus calculated to be 0.13 lb-sec/in (23 N-sec/m) and 216 lb/in ($3.78(10^4)$ N/m) respectively.

The FRF, curve fit and coherence at point 1z for the damping addition to the structure is shown in figure 4.11. A relatively large amount of damping was expected as the time

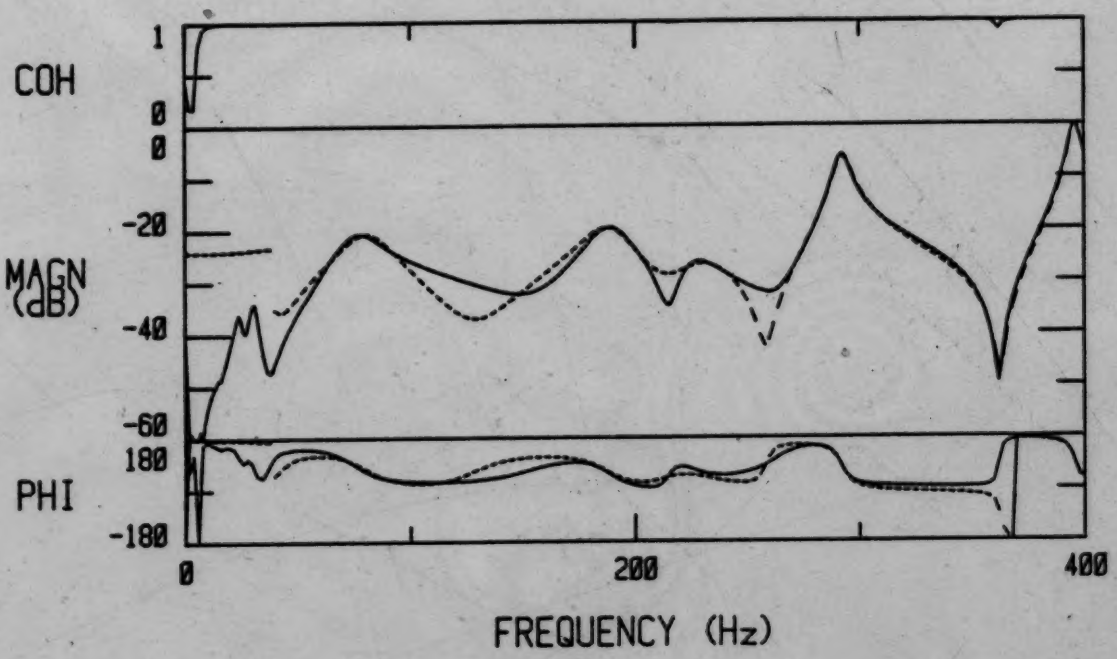

Figure 4.11 FRF and Coherence for the Damping Modified Structure at Test Point 1z

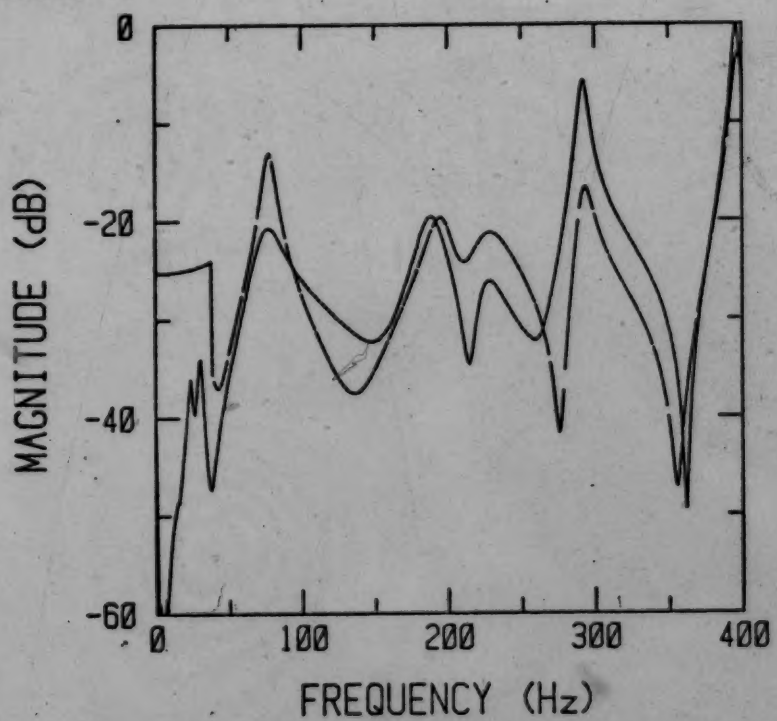

Figure 4.12 Damping Modified Structure Synthesis Plot

response waveforms decayed in a fraction of the total time period. The high modal damping is again indicated by the wider peaks and obvious modal coupling as shown in the figure. While the curve fit was relatively good at point 1z, at most other points the fit was much worse. This difficulty is simply attributed to a limitation of this type of fit. It is not known if other curve fitting algorithms suffer the same limitations for high modal damping because of a lack of documentation in this area. This is perhaps due to the fact that most structures considered do not have such a high degree of damping.

In modelling the change with SDM, it was again found that the additional mass and stiffnesses in the x and y directions played negligible roles in the dynamic behavior. It was assumed as well that damping in the x and y directions were also negligible for this type of mount. Thus the only modifications were those of damping and stiffness in the z direction between points 3 and 19. The compared results for the complex frequencies are shown in table 4.9. The predicted mode shapes are once again summarized in tables 4.10-4.14. The frequency test values from table 4.9 for this modification are averaged values obtained at points where the curve fit appeared to conform closely to the experimental data. The table displays good agreement for the natural frequencies since they are most dependent on the stiffness modification, not the damping. The damping is much less consistent with a large discrepancy in the first mode.

In order to investigate the effects of possible variations in the experimental value of the damping constant, ±20 % deviation in c was used to make predictions. These results, together with the original prediction and test results are shown in table 4.8. It can be seen that the damping in particular modes draws further away from the test values for both the higher and lower values of the damping coefficient. Therefore, it appears that the error in the damping coefficient cannot account for the effects discussed above.

The synthesis plot for point 1z is shown in figure 4.12. As can be seen, the differences between predicted and actual FRF amplitudes is much more than in the previous modifications.

The test structure and EMA data acquisition set-up are shown in plate 4.1.

MODE	PARAMETER	TEST	-20%	ORIGINAL PREDICTION	+20%
1	FREQ (Hz)	78.7	77.6	77.8	78.0
	DAMP (%)	14.2	3.8	5.1	6.4
2	FREQ (Hz)	188.7	194.2	196.0	198.7
	DAMP (%)	4.9	3.7	4.8	5.6
3	FREQ (Hz)	226.6	227.7	225.4	222.0
	DAMP (%)	5.4	5.2	7.1	9.4
4	FREQ (Hz)	292.2	293.2	292.4	291.5
	DAMP (%)	1.1	1.3	1.6	1.8
5	FREQ (Hz)	395.9	397.3	396.9	396.5
	DAMP (%)	0.5	0.5	0.7	0.9

Table 4.8 Effects on Prediction of a $\pm$ 20% Variation in the Experimental Damping Constant

MODE	PARAMETER	ORIGINAL STRUCTURE	MASS MOD.		STIFFNESS MOD.		DAMPING MOD.	
			TEST	SDM	TEST	SDM	TEST	SDM
1	FREQ (Hz)	48.2	42.5	39.6	105.8	104.9	78.7	77.8
	DAMP (%)	0.9	2.0	0.8	0.2	0.4	14.2	5.1
2	FREQ (Hz)	171.3	128.7	120.7	204.8	207.3	188.7	196.0
	DAMP (%)	0.1	0.1	0.1	0.2	0.2	4.9	4.8
3	FREQ (Hz)	217.9	187.4	198.1	282.4	282.1	226.6	225.4
	DAMP (%)	0.2	0.2	0.2	0.1	0.1	5.4	7.1
4	FREQ (Hz)	290.8	271.8	271.0	379.2	384.0	292.2	292.4
	DAMP (%)	0.2	0.1	0.1	0.1	0.1	1.1	1.6
5	FREQ (Hz)	395.8	383.2	383.0	--	1019.2	395.9	396.9
	DAMP (%)	0.1	0.1	0.1	--	0.0	0.5	0.7

Table 4.9 Summary of Predictions and Tests of Modification

TEST POINT	ORIGINAL STRUCTURE	MASS MOD. PREDICTION	STIFFNESS MOD. PREDICTION	DAMPING MOD. PREDICTION
1	28.8	27.5	-39.7	-34.2
2	27.4	27.9	-17.7	-24.4
3	26.0	28.2	3.5	-14.9
4	23.6	22.0	-38.9	-30.7
5	20.7	20.8	-15.4	-19.3
6	21.2	23.0	3.7	-11.9
7	17.0	15.1	-36.4	-25.6
8	14.4	14.2	-14.6	-15.1
9	14.2	15.4	3.2	- 7.8
10	10.1	8.1	-32.1	-19.7
11	8.6	8.2	-11.0	-10.0
12	7.8	8.6	3.3	- 3.7
13	3.2	2.9	- 5.4	- 4.4
14	3.0	3.4	2.5	- 1.0
15	- 0.7	- 0.8	0.5	0.7
16	0.2	0.1	- 0.8	- 0.5
17	0.2	0.3	1.3	0.3
18	- 5.8	- 5.8	5.1	5.8
19	- 5.6	- 5.6	4.4	5.3

Table 4.10 Mode 1 Mode Shapes for the z Direction

TEST POINT	ORIGINAL STRUCTURE	MASS MOD. PREDICTION	STIFFNESS MOD. PREDICTION	DAMPING MOD. PREDICTION
1	31.0	40.3	4.5	18.3
2	- 5.0	6.5	2.3	- 3.5
3	-40.8	-26.0	- 3.5	-27.2
4	34.4	42.6	2.2	18.5
5	- 2.3	7.7	- 0.9	- 3.9
6	-36.9	-23.0	- 6.1	-26.8
7	36.3	43.2	- 0.6	17.6
8	2.0	10.8	5.2	- 4.2
9	-28.5	-17.2	- 7.4	-23.0
10	36.7	41.5	- 1.5	17.3
11	3.0	9.6	- 5.2	- 3.4
12	-21.2	-12.4	- 9.4	-19.6
13	1.9	5.4	- 3.8	- 2.4
14	-12.6	- 6.9	- 8.9	-13.5
15	1.5	- 0.2	5.3	3.8
16	0.4	1.1	- 1.0	- 0.6
17	- 4.9	- 2.4	- 6.6	- 6.9
18	0.6	- 3.4	4.2	3.5
19	- 0.3	- 2.4	- 2.8	- 1.0

Table 4.11 Mode 2 Mode Shapes for the z Direction

TEST POINT	ORIGINAL STRUCTURE	MASS MOD. PREDICTION	STIFFNESS MOD. PREDICTION	DAMPING MOD. PREDICTION
1	10.2	- 4.5	31.3	28.1
2	- 7.1	- 3.6	17.3	- 9.1
3	-20.3	0.8	3.6	-44.3
4	13.9	- 3.6	16.6	29.4
5	- 2.6	- 1.5	3.4	- 7.3
6	-16.0	2.1	-10.2	-42.1
7	17.1	- 2.5	-17.7	28.8
8	4.0	1.7	-10.5	- 3.4
9	-10.5	2.6	-23.3	-35.3
10	17.7	- 2.7	-16.9	27.1
11	4.5	1.3	-20.0	- 3.3
12	- 4.0	4.8	-27.9	-26.5
13	3.4	1.2	-17.3	- 2.2
14	1.3	6.0	-21.0	-14.5
15	- 5.6	- 5.8	- 7.0	- 2.6
16	0.8	0.2	- 7.6	- 0.9
17	4.3	5.8	- 8.3	- 3.3
18	- 3.6	- 3.4	1.9	0.5
19	4.0	4.0	4.7	4.0

Table 4.12 Mode 3 Mode Shapes for the z Direction

TEST POINT	ORIGINAL STRUCTURE	MASS MOD. PREDICTION	STIFFNESS PREDICTION	DAMPING MOD. PREDICTION
1	25.4	29.4	24.6	-10.0
2	23.2	18.7	10.5	-26.7
3	20.5	7.2	- 4.7	-41.8
4	8.6	13.5	12.8	5.8
5	6.9	3.4	0.6	-10.8
6	4.3	- 7.9	-13.8	-25.9
7	-11.7	- 6.3	- 1.1	23.9
8	-10.2	-12.3	- 8.1	6.9
9	-12.9	-22.4	-20.1	- 6.6
10	-28.1	-21.8	- 9.6	38.1
11	-21.0	-22.0	-11.0	17.2
12	-21.7	-28.3	-18.1	6.4
13	-18.8	-18.6	- 3.7	16.4
14	-18.8	-22.0	- 7.5	10.5
15	- 7.0	- 5.5	7.5	5.7
16	- 8.6	- 7.7	5.2	8.1
17	- 8.8	- 9.3	3.6	7.3
18	2.2	2.7	- 4.0	- 2.2
19	3.7	3.9	- 2.5	- 1.3

Table 4.13 Mode 4 Mode Shapes for the z Direction

TEST POINT	ORIGINAL STRUCTURE	MASS MOD. PREDICTION	STIFFNESS MOD. PREDICTION	DAMPING MOD. PREDICTION
1	25.8	18.6	- 4.8	-24.6
2	20.1	12.0	-32.2	-27.2
3	12.6	3.5	-57.2	-27.2
4	9.0	6.5	11.2	- 4.7
5	5.2	1.6	-16.3	- 8.9
6	- 1.5	- 6.1	-41.8	- 9.9
7	-10.5	- 7.4	28.5	-18.1
8	- 9.2	- 8.0	1.3	9.3
9	-14.1	-13.6	-22.1	7.3
10	-23.0	-15.3	40.8	33.2
11	-15.0	-10.7	10.0	17.2
12	-16.5	-13.3	- 8.3	13.6
13	- 7.3	- 3.3	8.6	9.8
14	- 8.0	- 4.9	- 1.5	7.7
15	7.2	9.0	- 1.0	- 6.4
16	3.9	5.7	1.8	- 2.5
17	2.8	4.1	0.1	- 2.0
18	- 4.2	- 3.8	2.5	4.1
19	- 3.3	- 3.7	4.1	3.8

Table 4.14 Mode 5 Mode Shapes for the z Direction

Plate 4.1 EMA Data Acquisition Set-Up and Test Structure

5. CONCLUSIONS AND FURTHER STUDIES

This study has shown how EMA and SDM can be combined to form a powerful tool in solving vibration problems. The prediction accuracy of modifications using SDM depends most highly on very good estimates of the original modal parameters from EMA since these form the modal model. The major inherent problems of noise and leakage contribute in reducing this accuracy so that the general case of complex modes is virtually impossible to accurately identify as such. As a result, a real mode model approximation was used where damping effects were taken into account through the assumption of proportional damping. Once the modal model had been constructed, accurate predictions using SDM were possible provided that the problems and limitations of the technique were realized. It was shown in chaper 3 how to reduce noise and leakage to improve the measurements. Noise greatly affects the measurements and thus predictions as displayed in the results obtained for the free-free beam. In using the modal model, it is important to realize that it is a truncated model with a frequency range set by the tests on the original structure. Thus, predictions far outside the scope of the model could not be expected to be accurate as shown in the fifth mode prediction for the stiffness modification to the cantilever structure. Also found was that for many situations, especially for beam structures, the rotary inertia effects become important as displayed in the mass prediction. In order to improve predictions in

these situations, rotational degrees-of-freedom must be estimated and added to the modal model. The final conclusion from this study was that damping effects at the best of times are difficult to predict since damping material properties typically vary a great deal, especially over frequency. In addition, the model used assumes proportional linear viscous damping. Therefore, damping modification predictions will ultimately be less accurate.

Additional problems not included in this study but still of considerable importance are those dealing with structural non-linearities and frequency resolution. When non-linearities are present in a structure, the excitation spectrum level must be precisely controlled and thus the transient method becomes unsuitable. In this situation, the other classes of excitation, namely random and sinusoidal signals are used. In the case of frequency resolution, the Zoom transform is employed to increase resolution by examination of discrete bands in the frequency range of interest. For the cantilever test structure used in this study, only frequencies up to 400 Hz were examined resulting in a very good frequency resolution of 1 Hz. However, in many situations, much higher frequencies are examined with a corresponding drop in frequency resolution and thus baseband resolution becomes inadequate.

In determining a more accurate modal model, especially over high frequencies or when there is a high degree of modal coupling, various improvements to the present

technique could be developed. These include the implementation of the Zoom transform and further investigation into improvement of the curve fitting algorithm.

Further studies in the area of structural modifications might include modifications, especially damping modifications using a complex mode model like that described in O'Callahan and Avitabile [17] or using direct modification from FRF's as shown in reference [5]. Comparison of these techniques for various modifications and substructuring could yield further insight in this area.

Extensions to uses of the modal model and SDM include forced response simulation and stress prediction. Both these techniques rely on the fact that the FRF completely describes a structures dynamics. Forced response simulation involves the determination of the response of the structure by multiplying the system FRF by a synthesized forcing function. Stress prediction combines the system FRF with Fourier transformed strain gauge operating time domain data to calculate a system 'pseudo' forcing function. A modified FRF found from using SDM can then be multiplied by the 'pseudo' forcing function to obtain modified system stresses.

REFERENCES

1. Brigham, E.O., *The Fast Fourier Transform*, Prentice-Hall Inc., Englewood Cliffs, New Jersey; 1974

2. Brown, D.L., Allemang, R.J., Riehle, P.J. and Yasuda, C., "An Estimation Method For Rotational Degrees of Freedom Using a Mass Additive Technique", Proceedings of the Second International Modal Analysis Conference, pp. 877-886; 1984

3. Brown, D.L., Allemang, R.J., Zimmerman, R. and Mergeay, M., "Parameter Estimation Techniques for Modal Analysis", SAE paper #790221, 19 pp.; 1979

4. Corelli, D., "Ratio Calibration - the Right Choice for Modal Analysis", Sound and Vibration, Vol. 18, No. 1; 1984

5. Crowley, J.R., Klosterman, A.L., Rocklin, G.T. and Vold, H., "Direct Sructural Modification using Frequency Response Functions", Proceedings of the Second International Modal Analysis Conference, pp. 58-65; 1984

6. Formenti, D. and Welaratna, S., "Structural Dynamics Modification - An Extension to Modal Analysis", SAE paper #811043, 23 pp.; 1981

7. Fyfe, K., "Practical Implementation of Modal Analysis", M.Sc. Thesis, University of Alberta, Mechanical Engineering Department; 1983

8. Hallquist, J., "Modification and Synthesis of Large Dynamic Structural Systems", Ph.d. Dissertation, Michigan Technological University, 1974

9. Hallquist, J., and Snyder, V.W., "On the Connection of Viscously Damped Continuous Vibratory Systems", Journal of Sound and Vibration, 32(1), pp. 131-142; 1974

10. Halvorsen, W.G. and Brown, D.L., "Impulse Technique for Structural Frequency Response Testing", Sound and Vibration, pp. 8-21; November 1977

11. Herbert, M.R., and Kientzy, D.W., "Applications of Structural Dynamics Modification", SAE paper, #801125, 7 pp.; 1981

12. Ibrahim, S.R. and Lin, L.C., "The Use of Complex Versus Normal Modes in Structural Model Improvement", Proceedings of the Second International Modal Analysis Conference, pp. 415-424; 1984

13. James, M.L., Smith, G.M. and Wolford, J.C., *Applied Numerical Methods for Digital Computation*, second edition, Harper and Row Publishers Inc.; 1977

14. Kron, G., *Diakoptics*, Macdonald, 1963

15. Levy, E.C., "Complex Curve Fitting", IRE Transactions on Automatic Control, Vol. AC-4, pp. 37-44; May 1959

16. MacDuff, J.N. and Curreri, J.R., *Vibration Control*, McGraw - Hill Book Company Inc.; 1958

17. O'Callahan, J. and Avitabile, P., "A Structural Modification Procedure Using Complex Modes", Proceedings of the First International Modal Analysis Conference, pp. 167-181; 1982

18. Pomazal, R., "The Effect of Local Modification on the Eigenvalues and Eigenvectors of Damped Linear Systems", Ph.d. Dissertation, Michigan Technological University, 1969

19. Potter, R., and Richardson, M., "Mass, Stiffness and Damping Matrices from Measured Modal Parameters", ISA Conference and Exhibit, New York City; October 1974

20. Powell, C.D., "Experimental Modal Analysis With Structural Modification Applied to System Stress Prediction", (abstract only), Proceedings of the First International Modal Analysis Conference, pp. 417; 1982

21. Ramsey, K.A., "Effective Measurements for Structural Dynamics Testing - Part 1", Sound and Vibration, Vol. 9, No. 11; 1975

22. Ramsey, K.A., "Effective Measurements for Structural Dynamics Testing - Part 2", Sound and

Vibration, Vol. 10, No. 4; 1976

23. Ramsey, K.A. and Firmin, A., "Experimental Modal Analysis, Structural Modifications and FEM analysis - Combining Forces on a Desktop Computer", Proceedings of the First International Modal Analysis Conference, pp. 443-455; 1982

24. Richardson, M., "Modal Analysis Using Digital Test Systems", Seminar on Understanding Digital Control and Analysis in Vibration Test Systems, Shock and Vibration Information Center Publication, pp. 43-64; May 1975

25. Richardson, M.H. and Formenti, D.L., "Parameter Estimation from Frequency Response Measurements Using Rational Fraction Polynomials", Proceedings of the First International Modal Analysis Conference, pp. 167-181; 1982

26. Richardson, M. and Potter, R., "Identification of the Modal Parameters of an Elastic Structure from Measured Transfer Function Data", Twentieth International Instrumentation Synposium, Albaquerque, New Mexico; May 21-23, 1974

27. Sanathanan, C.K. and Keorner, J., "Transfer Function Synthesis as a Ratio of Two Complex Polynomials", IEEE Transactions on Automatic Control, pp. 56-58; January 1963

28. Simpson, A. and Tabbarok, B., "On Kron's Eigenvalue Procedure and Related Methods of Frequency Analysis", Quarterly Journal of Mechanics and Applied Mathematics, Vol. 21, Part 1, pp. 1-39; 1968

29. Smiley, R.G. and Brinkman, B.A., "Rotational Degrees of Freedom in Structural Modification", Proceedings of the Second International Modal Analysis Conference, pp. 937-939; 1984

30. Vierck, R.K., *Vibration Analysis*, Thomas Y. Crowell Harper and Row Publishers, New York; 1979

31. Weissenburger, J.T., "Effects of Local Modifications on the Vibration Characteristics of Linear

Systems", Journal of Applied Mechanics, Vol. 35, Trans. ASME, Series E., Vol. 90, No. 2, pp. 327-332; 1968

32. Zienkiewicz, O.C., *The Finite Element Method*, third edition, McGraw - Hill, London; 1977

33. "Improving the Accuracy of Structural Response Measurements", Hewlett Packard Application Note No. 204-2

34. "The Fundamentals of Signal Analysis", Hewlett Packard Application Note No. 243